

Phase Field Modelling of Mode III Dynamic Fracture

A Project Report
Submitted in Partial Fulfillment of the
Requirement for the Degree of
Master of Engineering
in
Materials Engineering

by
Akash Bhattacharjee

Supervisor
Dr. Abhik Choudhury



Materials Engineering
Indian Institute of Science
Bangalore - 560012

June 2015

Declaration of Authorship

I, Akash Bhattacharjee, declare that this thesis titled, **Phase Field Modelling of Mode III Dynamic Fracture** and the work presented in it are my own. I confirm that:

- This work was done wholly or mainly while in candidature for a research degree at this University.
- Where any part of this thesis has previously been submitted for a degree or any other qualification at this University or any other institution, this has been clearly stated.
- Where I have consulted the published work of others, this is always clearly attributed.
- Where I have quoted from the work of others, the source is always given. With the exception of such quotations, this thesis is entirely my own work.
- I have acknowledged all main sources of help.

Signed:

Date:

Acknowledgements

I would like to express my deepest respect and gratitude to my ME thesis advisor Dr. Abhik Choudhury for guiding me though out the year.. I am grateful to him for giving me opportunity to work in entirely new area of phase field methods.

I would like to thank Professor Vikram Jayaram (chairman) and Professor Kamani Chattopadhyay (Divisional chairman) for providing all the facilities in carrying out this research work. I would like to thank Professor T. A. Abhinandan, Vikram Jayaram, Govind Gupta and Subodh Kumar for their valuable subject discussion in my project work. I would like to thank professor T. A. Abhinandan, D. Banerjee, S. Karthikeyan, Chandan Srivatsav, Rajiv Ranjan, Subodh Kumar, Alok Paul, Satyam Suwas for their valuable subject discussions and guidance in the ME course work.

I also thank the Materials Engineering staff and technicians who have helped me in carrying out my research work.

My sincere gratitude to all my colleagues in my group especially Arka, Bhalachandra, Aapar, Supriyo for their support and cooperation.

I would also like to thank my friends Amit, Manoj, Rishi, Nikki, Arunima, Abhishek, Abhijeet, Subodh, Devi Lal, Pushpendra, Rohit, Shobit, Tushar, Surya, Urbi, Shankha for their supprot and motivation.

I would also like to thank all my team mates of IISc cricket team and our Department cricket team for their support and belief.

I would like to mention my B.Tech friends Ashutosh Choudhary, Prashant Bighane, Ashwin Gajghate, Digvjay Patil, Jayant Barode, Kushal Gupta, Ketan Lanjewar, Nipun Agrawal and other.

I would also like to mention Rahul, Saurabh, Bhishma, Suraj, Ankit.

I would like to thank my family for their support and motivation though out my life.

....

Contents

| | |
|---|-----|
| Declaration of Authorship | i |
| Acknowledgements | ii |
| Contents | iii |
| List of Figures | v |
| 1 Introduction | 1 |
| 1.1 Phase Field | 1 |
| 1.2 Fracture and Phase Field | 3 |
| 2 Basic Aspects of Fracture | 4 |
| 2.1 Griffith's theory | 4 |
| 2.2 Energy Release Rate | 6 |
| 2.3 Stress at crack tip | 7 |
| 2.4 Modes of Fracture | 7 |
| 2.4.1 MODE III Crack | 8 |
| 3 Mathematical Model | 11 |
| 3.1 The Basic Model | 11 |
| 3.2 Anisotropic Shear Modulus | 14 |
| 3.3 Multi Grains | 18 |
| 4 Solving Techniques | 19 |
| 4.1 Explicit Scheme | 19 |
| 4.1.1 Discretization of the Model | 20 |
| 4.1.1.1 Boundary Conditions | 23 |
| 4.1.2 Discretization of the Anisotropic Model | 23 |
| 4.1.2.1 To calculate $a_c^2(n)$ | 23 |
| 4.1.2.2 To calculate $\nabla_i \left[\frac{\partial}{\partial \nabla \phi} a_c^2(n) \right]$ | 24 |
| 4.1.2.3 Discretization of $aniso_x$ | 24 |
| 4.1.2.4 Discretization of $aniso_y$ | 25 |
| 4.1.2.5 Boundary Conditions | 27 |
| 4.1.3 Discretization of Multi Grain Model | 27 |
| 4.1.3.1 Boundary Conditions | 28 |
| 4.2 Implicit Scheme | 28 |

| | | |
|----------|--|-----------|
| 4.2.1 | Douglas Scheme | 29 |
| 4.2.2 | Thomas Tridiagonal Method | 30 |
| 4.2.3 | Boundary Conditions | 32 |
| 5 | Results and Discussions | 33 |
| 5.1 | Introduction | 33 |
| 5.2 | Non-dimensionalization | 33 |
| 5.3 | Critical Delta | 34 |
| 5.4 | Comparison with Griffith's Model | 37 |
| 5.5 | Stress in front of Crack Tip | 38 |
| 5.6 | Crack Splitting | 40 |
| 5.7 | Crack Propagation in systems with different Shear Modulus | 40 |
| 5.8 | Crack Propagation in Linearly Toughened Material | 41 |
| 5.8.1 | Interaction of multiple cracks in the domain | 44 |
| 5.9 | Crack Propagation in Anisotropic Domain | 49 |
| 5.9.1 | Constant μ_0 | 50 |
| 5.9.2 | Linearly increasing μ_0 | 51 |
| 5.10 | Crack Propagation in Multi Grain System | 53 |
| 5.10.1 | Crack Splitting around hard grain in Multi-Grain System | 55 |
| 5.10.2 | Crack Path blocked by a Hard Grain | 56 |
| 5.10.3 | Crack Propagation in stacked phases | 57 |
| 5.10.3.1 | Linearly increasing Shear Modulus of both α and β phase | 60 |
| 5.10.3.2 | Linearly decreasing Shear Modulus of α phase and linearly increasing Shear Modulus of β phase | 61 |
| 6 | Future Work | 64 |

List of Figures

| | |
|---|----|
| 1.1 a) Sharp Interface. b) Diffused Interface. | 2 |
| 2.1 Static plane-crack system, showing incremental extension of crack length a through da; P is applied load. | 4 |
| 2.2 Central crack of length 2a. | 5 |
| 2.3 Different modes of fracture. | 8 |
| 2.4 Polar co-ordinates of point P near crack tip C. | 9 |
| 3.1 Effective potential plot with $\epsilon_c = 0.65$, $\epsilon_0 = 0.0004$ and $\mu = 1.0$ | 13 |
| 3.2 Polar plot of anisotropic Shear Modulus. | 15 |
| 3.3 Grained structure of the material. | 18 |
| 4.1 Discretization of the domain for calculating the Laplacian of ϕ . | 20 |
| 4.2 Discretization of domain for calculating the gradient of u . | 21 |
| 4.3 Discretization of the domain, first distretizing domain for the displacement and then for $g(\phi)$ to finally find $\vec{\nabla} \cdot (g(\phi) \vec{\nabla} u)$ | 22 |
| 4.4 Discretization to calculate $\nabla \phi_x$ and $\nabla \phi_y$ using central difference method. | 24 |
| 4.5 Discretization of matrix to calculate $\nabla \phi_y$ for $aniso_x$. | 25 |
| 4.6 Discretization of matrix to calculate $\nabla \phi_x$ for $aniso_x$. | 25 |
| 4.7 Discretization of matrix to calculate $\nabla \phi_x$ for $aniso_y$. | 26 |
| 4.8 Discretization of matrix to calculate $\nabla \phi_y$ for $aniso_y$. | 26 |
| 4.9 Discretization of the matrix for the anisotropy term. | 26 |
| 4.10 Discretization of the domain for solving the displacement field. | 28 |
| 5.1 Change in velocity with delta giving an equilibrium point. | 35 |
| 5.2 Crack growing above the critical delta ($\Delta = 4$). | 36 |
| 5.3 Crack shrinking below the critical delta ($\Delta = 3.345$). | 36 |
| 5.4 Velocity of crack propagation at delta = 4. | 36 |
| 5.5 Steady state crack propagation. | 37 |
| 5.6 Shear stress applied to a sample containing crack. | 37 |
| 5.7 Different critical displacement for different domain length. | 38 |
| 5.8 Crack propagating in a domain. | 39 |
| 5.9 Stress in front of the crack tip. | 39 |
| 5.10 Crack splitting at higher applied displacement. | 40 |
| 5.11 Crack propagation velocities comparison in system having different shear modulus. | 41 |
| 5.12 Contour plot of linearly increasing shear modulus in the domain. | 42 |
| 5.13 a) Initial domain containing a cracks at the left most end of matrix. b) Propagation of the cracks under linear gradient of shear modulus. | 42 |

| | | |
|------|---|----|
| 5.14 | Crack propagation velocity for the crack propagating in the direction of increasing shear modulus. | 43 |
| 5.15 | a) Initial domain containing a cracks at the right most end of matrix. b) Propagation of the cracks under linear gradient of shear modulus. | 43 |
| 5.16 | Crack propagation velocity for the crack propagating in the direction of decreasing shear modulus. | 44 |
| 5.17 | Sequence of crack propagation from either end of domain at the applied stress of 0.45 units. | 45 |
| 5.18 | Sequence of crack propagation from either end of domain at the applied stress of 0.5 units. | 46 |
| 5.19 | Sequence of crack propagation for horizontally away initiated cracks at the applied stress of 0.4 units. | 47 |
| 5.20 | Sequence of crack propagation for horizontally away initiated cracks at the applied stress of 0.45 units. | 48 |
| 5.21 | Sequence of crack propagation for horizontally away initiated cracks at the applied stress of 0.5 units. | 49 |
| 5.22 | Polar plot of anisotropic Shear Modulus. | 50 |
| 5.23 | Crack branching in anisotropic domain under the applied stress of 0.5 units. | 50 |
| 5.24 | Crack branching in anisotropic domain under the applied stress of 0.55 units. | 51 |
| 5.25 | Crack branching in anisotropic domain under the applied stress of 0.5 units. | 52 |
| 5.26 | Crack branching in anisotropic domain under the applied stress of 0.6 units. | 52 |
| 5.27 | Crack branching in anisotropic domain under the applied stress of 0.7 units. | 53 |
| 5.28 | Sequence of crack propagating through a multi-grain system. | 54 |
| 5.29 | Sequence of crack propagating and splitting around a hard grain in a multi-grain system. | 55 |
| 5.30 | Sequence of two crack propagating in a multi-grain system and one crack path is blocked by a hard grain. | 56 |
| 5.31 | Domain containing alternately stacked α and β phases. | 57 |
| 5.32 | The velocity of crack propagation in alternately stacked phases. | 58 |
| 5.33 | The average velocity in a particular phase of the crack propagation in stacked phases. | 58 |
| 5.34 | The variation of crack length propagated in a fixed amount of time for different thickness of alternate α and β phases. | 59 |
| 5.35 | Domain containing alternately stacked α and β phases. | 60 |
| 5.36 | The velocity of crack propagation in alternately stacked phases. | 61 |
| 5.37 | The average velocity in a particular phase of the crack propagation in stacked phases. | 61 |
| 5.38 | Domain containing alternately stacked α and β phases. | 62 |
| 5.39 | The velocity of crack propagation in alternately stacked phases. | 62 |
| 5.40 | The average velocity in a particular phase of the crack propagation in stacked phases. | 63 |

Chapter 1

Introduction

1.1 Phase Field

In materials science there are many problems which involve movement of phase boundaries coupled with transport of heat, mass and momentum across the interfaces as well as in the bulk. These problems are classified as free-boundary or alternatively moving boundary problems. Examples of such problems are solidification, phase separation, order-disorder transformation etc. All these phenomena involve the re-distribution of an extrinsic property across the interface between the different homogeneous entities also called phases. Herein, the phase-field method is extensively used to solve such problems which allow for the imposition of boundary conditions at non-stationary interfaces, without the explicit requirement of tracking the interface. Additionally, deterministic self-consistent evolution laws for the phase-fields can be constructed which can describe complex geometric evolution involving multiple curvatures and catastrophic phase evolution. Furthermore, the models and therefore their implementation can be generally formulated irrespective of the dimensionality. Traditionally, solidification has been one phenomena which has been widely studied using the phase-field method [3]. Thereafter, the method has evolved in order to consider other problems wherein there is coupling of elastic and magnetic fields [4].

The general framework of the phase-field method involves the construction of an artificial interface between the different phases with a prescribed width. The state of the complete system is represented continuously by a variable known as the phase-field order parameter, ϕ , which varies smoothly across the interface(Figure 1.1 b)). The order parameter takes distinct values in different phases (suppose 1 and 0 for the case of two phases), with a smooth change between the different values across the interface. The

spatio-temporal evolution of the interface describes the evolution of the phases and are governed by partial differential equations with appropriate boundary conditions.

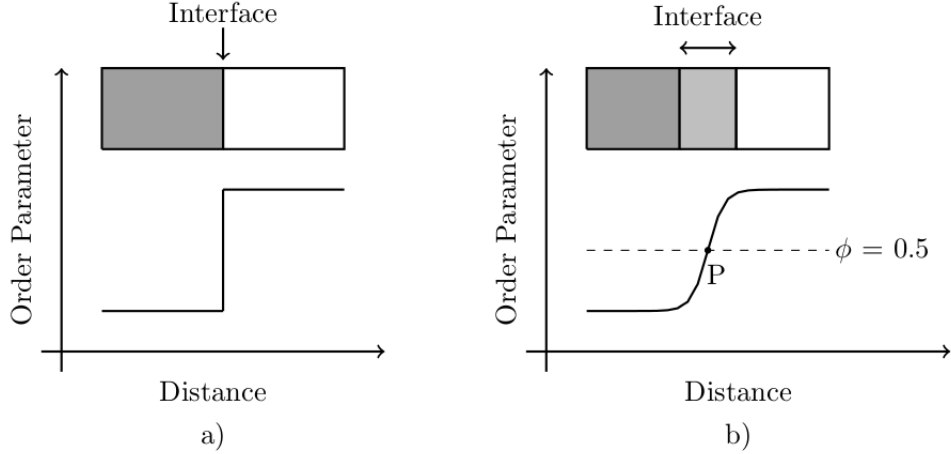


Figure 1.1: a) Sharp Interface. b) Diffused Interface.

The evolution of phases with time is assumed to be proportional to the variation of the free energy function with respect to the order parameter [5]

$$\frac{\partial \phi}{\partial t} = M \frac{\partial g}{\partial \phi}$$

where M is proportionality constant and g describes how the free energy of the system varies with the order parameter [5]. Therefore g is given as follows:

$$g = \int_V [g_0\{\phi\} + \epsilon(\nabla\phi)^2]dV$$

where V represents the volume of the system. The first term is the sum of free energy of both the phases present in the system and may also contain the activation barrier across the interface. The second term depends only on the gradient of ϕ , and therefore it is non-zero only at the interface where there is transition between two phases and it describes the interfacial energy of the interface.

Mathematically we require the interface between the phases to have a certain width(2λ) so that continuous change in ϕ across the interface can be achieved. The choice of the width is essentially determined by the smallest principal morphological length scale. Naturally, the computational effort scales with this choice of interface width as,

$$\frac{t}{t_0} \propto \left(\frac{\lambda}{\lambda_0}\right)^{-D}$$

where D represents the dimension of the simulation and t is the computational time. t_0 and λ_0 are the constants. Therefore as the width of the interface increases, the

computational resources required reduces, but at the same time the there is a possibility of loss of details at the interface.

1.2 Fracture and Phase Field

Phase field technique which was originally introduced to simulate and solve the kinetics of phase transitions, is now extended to solve the problem of the dynamics of crack propagation. In general phase field methods the order parameter is used to distinguish between different phases, such as solid and liquid, but for modeling of cracks, such an order parameter distinguishes between the solid phase and the broken state inside the crack. As usual in the phase field context, the order parameter changes smoothly between the states at the crack surfaces. The crack growth then become conceptually comparable to the front propagation in the first order phase transition.

The uniform motion of a crack is relatively well understood in the framework of continuum theories. Here, the conventional approach is to treat the crack as a front or interface separating broken and unbroken regions of the material and the propagation is governed by the balance of the elastic forces in the materials and cohesive stresses near the crack tip.

Chapter 2

Basic Aspects of Fracture

2.1 Griffith's theory

Griffith's criteria is the basis of fracture of brittle materials. Griffith simply tried to find the equilibrium configuration that will minimize the free energy of the system and hence obtain the equilibrium configuration of the system [6]. Griffith considered a isolated crack in a solid which is subjected to applied stress and formulated the criteria for crack extension using the fundamental energy theorem of classical mechanics and thermodynamics. The total energy of this system consists of the elastic strain energy (U_E) and the surface energy (U_S), and the equilibrium is achieved by balancing the total energy (U_{total}) over a virtual crack extension.

$$U_{total} = U_E + U_S$$

As the crack increases the stored elastic strain energy of the system decreases whereas the surface energy increases as new crack surfaces are created.

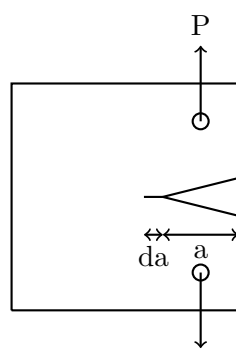


Figure 2.1: Static plane-crack system, showing incremental extension of crack length a through da ; P is applied load.

According to Griffith energy balance concept, equilibrium is achieved when,

$$\frac{dU_{total}}{da} = 0$$

And the Griffith criteria states that crack will grow if the rate of release of stored elastic strain energy from its growth is more than the rate at which the surface energy of the crack is increased.

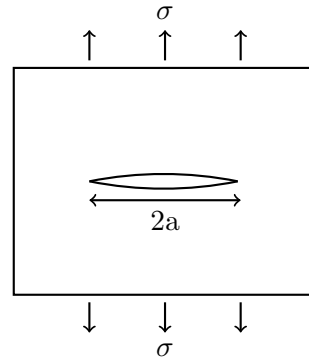


Figure 2.2: Central crack of length \$2a\$.

For a elastic system containing elliptical central crack of length \$2a\$ and under tensile stress field of \$\sigma\$ at the ends, the of the stored elastic strain energy is given by,

$$U_E = \frac{\pi a^2 \sigma^2}{E'}$$

where \$E'\$ is the Young's modulus in plane stress condition (thin plate), and \$E/(1 - \nu^2)\$ in plane strain (thick plate) condition with \$\nu\$ being Poisson's ratio. The surface energy of the crack system is given as,

$$U_S = 4a\gamma$$

where \$\gamma\$ is the free surface energy of the system. The total energy of the system becomes,

$$U_{total} = U_E + U_S$$

$$U_{total} = -\frac{\pi a^2 \sigma^2}{E'} + 4a\gamma$$

\therefore According to the Griffith's criteria at equilibrium (i.e. $dU_{total}/da = 0$), if $\sigma = \sigma_c$ and $a = a_c$, then the critical stress is given by

$$\sigma_c = \left(\frac{2E'\gamma}{\pi a_c} \right)^{1/2}$$

This σ_c is the equilibrium critical stress and a_c is the equilibrium critical crack length. If the applied stress is less than the critical stress (σ_c) then the crack will not be affected, but if the applied stress is more than the critical stress then the crack starts to grow.

2.2 Energy Release Rate

Griffith stated that the crack will grow only when the energy released during crack growth is sufficient to provide the energy required for creation of new surface during crack growth [7].

$$i.e. \frac{dU}{da} = \frac{dW}{da}$$

where U is the elastic energy and W is the energy required for crack growth. And dU/da is calculated as,

$$\frac{dU}{da} = \frac{2\pi\sigma^2 a}{E'}$$

and in this equation, dU/da is replaced by

$$G = \frac{\pi\sigma^2 a}{E'}$$

where G is called "elastic energy release rate" per crack tip. G is also called the crack driving force, having units of energy per unit thickness per unit crack extension or force per unit crack extension.

And energy consumed by crack extension is surface energy and it is constant. And in order for crack to propagate the G should be greater than the surface energy. Therefore there is a critical value of G above which the crack will only grow, and is given by,

$$G_c = \frac{\pi\sigma_c^2 a}{E'} = 2\gamma$$

here G_c is the critical energy release rate. This critical energy release rate is the characteristics surface energy of the material, and G_c replace the thermodynamic surface energy used in the calculation. G_c is also referred as the work required to produce unit increase in crack area. There are three possibilities as mentioned below;

- If the energy release rate is lower than the critical energy release rate ($G < G_c$) then the crack is stable.
- Conversely, if $G > G_c$ then the crack will grow.
- But if both energy release rate and critical energy release rate are equal ($G = G_c$), the the crack is in metastable equilibrium.

2.3 Stress at crack tip

Crack growth in materials undergoing brittle fracture is governed by the stress field around the crack tip and other material properties that resist crack growth. Near the crack tip the stress has a universal singular behavior in the framework of the linear theory of elasticity [7] , given by,

$$\sigma_{ij}^m = \frac{K}{\sqrt{2\pi r}} f_{ij}^m(\theta)$$

where $f_{ij}^m(\theta)$ is the function of r and θ of the point for which stress is calculated away from the crack tip and K is the stress intensity factor, which provides the state of stress near the crack tip caused by remote loads or residual stress. The magnitude of K depends on sample geometry, the size and location of the crack, and the magnitude and the modal distribution of loads on the material.

The stress intensity factor is linearly related to the applied stress and to the square root of the characteristics length which is the crack length.

$$\text{i.e. } K = \sigma \sqrt{\pi a}$$

This stress intensity factor amplifies the magnitude of applied stress using the geometry parameter. There is a critical value of this stress intensity factor above which only the crack propagates, and this is called critical stress intensity factor (K_c).

Energy release rate is also related to stress intensity factor as,

$$G = \frac{K^2}{E'}$$

2.4 Modes of Fracture

A crack is made up of two surfaces which are initially assumed to be in the same plane, and the relative movement of one surface with respect to other causes the crack front to

move. There are three independent relative movement possible and they corresponds to three different modes of fracture [7]. These modes of fracture are called Mode I, Mode II and Mode III (Figure 2.3), and any fracture can be represented by one or more of these modes.

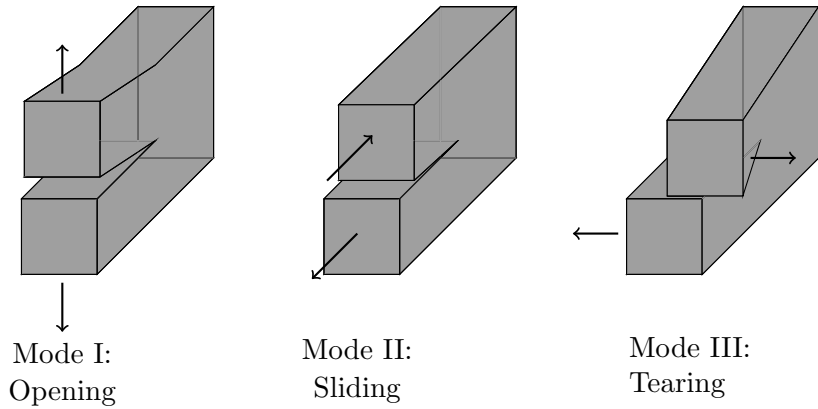


Figure 2.3: Different modes of fracture.

Mode I (Opening): The displacement is applied in y direction such that the crack surfaces move away in a plane perpendicular to the crack plane, such that the crack opens up.

Mode II (Sliding) : The displacement is applied in x direction such that the crack surfaces slides over each other in the direction parallel to the crack front.

Mode III (Tearing) : The displacement is applied in z direction such that the crack surfaces are sheared out of the plane in the direction parallel to the crack front. This causes a tearing action in the crack surfaces.

2.4.1 MODE III Crack

The mode III fracture is a out of plane shear deformation [7], and for this the displacements are given as

$$u_x = 0$$

$$u_y = 0$$

$$u_z = w$$

And thus the shear strains produced are given as,

$$e_{xz} = \frac{1}{2} \frac{\partial w}{\partial x} \quad \text{and}$$

$$e_{yz} = \frac{1}{2} \frac{\partial w}{\partial y}$$

And the corresponding stress according to the Hooke's law are given as

$$\sigma_{xx} = \sigma_{yy} = \sigma_{zz} = 0$$

$$\tau_{xz} = 2\mu e_{xz} \quad \text{and}$$

$$\tau_{yz} = 2\mu e_{yz}$$

The equilibrium equation for the this case reduces to

$$\frac{\partial \tau_{xz}}{\partial x} + \frac{\partial \tau_{yz}}{\partial y} = 0$$

which can be easily be written in terms of displacement as

$$\nabla^2 u_z = 0$$

$$\therefore \nabla^2 w = 0$$

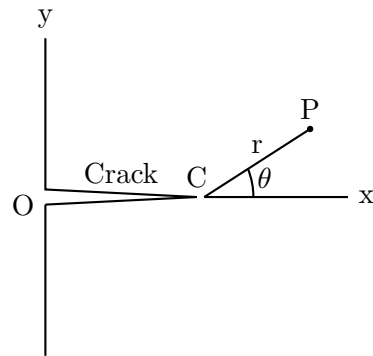


Figure 2.4: Polar co-ordinates of point P near crack tip C.

The stress field around the crack tip is given as,

$$\tau_{xz} = \frac{K_{III}}{\sqrt{2\pi r}} \sin\left(\frac{\theta}{2}\right)$$

$$\tau_{yz} = \frac{K_{III}}{\sqrt{2\pi r}} \cos\left(\frac{\theta}{2}\right)$$

and the displacement field around the crack tip is given as,

$$u_z = \frac{K_{III}}{\mu} \sqrt{\frac{r}{2\pi}} \sin\left(\frac{\theta}{2}\right)$$

where r and θ are the polar coordinates of the point (Figure 2.4) away from the crack tip where the shear stress and displacements are calculated. K_{III} is the stress intensity factor for the Mode III fracture and μ is the shear modulus.

Chapter 3

Mathematical Model

3.1 The Basic Model

The classical approach to solve the problem of brittle fracture is to solve the linear elastic equations with boundary conditions providing the driving stresses. But the linear continuum elasticity breaks down in the region very close to crack tip or the "process zone", as the solution have stress field which become singular at the crack tip. So it fails to predicts the instabilities of the tip dynamics. So in order to create a sensible framework for fracture mechanics one must use the microscopic theory at the crack tip along with the macroscopic physics elsewhere.

Alain Karma et al. [1] constructed a continuum model that maintains rotational symmetry even inside the process zone. For the mode III fracture, the standard displacement field \vec{u} (which is out of the plane) is represented by a scalar field u . Hence the linear elastic energy of the system is given as

$$E = \int \frac{1}{2} \mu \vec{\epsilon}^2 d\vec{x}$$

where the strain is given by, $\vec{\epsilon} = \vec{\nabla}u$ and μ is the elastic constant or in this case shear modulus. The basic idea of this fracture model is that the system will contain a local state of either unbroken material ($|\vec{\epsilon}| < \epsilon_c$) or the broken state ($|\vec{\epsilon}| > \epsilon_c$) using a phase field $\phi(x, t)$, where ϵ_c is the critical strain above which the energy becomes strain independent and fracture occurs.

The phase field obeys the standard two-minimum Ginzburg-Landau equation with the relative energy of the two wells dependent on $\epsilon^2 - \epsilon_c^2$ and how this ϕ affects the elasticity equation can be obtained from the relaxation dynamics, $\tau \partial_t \phi = -\delta E / \delta \phi$, where the

energy E is given by

$$E = \int \left[\frac{1}{2} D_\phi (\vec{\nabla} \phi)^2 + W_{DW}(\phi) + \frac{\mu}{2} g(\phi) (\bar{\epsilon}^2 - \epsilon_c^2) \right] d\vec{x} \quad (3.1)$$

The energy of the system (eq. 3.1) consists of three energy terms. The first two terms together describes the interfacial energy and the third term describes the strain energy.

The exact phase field equation calculated by solving the above equations is

$$\tau \partial_t \phi(\vec{x}, t) = D_\phi \nabla^2 \phi - W'_{DW}(\phi) - \frac{\mu}{2} g'(\phi) (\bar{\epsilon}^2 - \epsilon_c^2) \quad (3.2)$$

where $W_{DW}(\phi)$ is the double well potential function given by

$W_{DW}(\phi) = \frac{1}{4} \phi^2 (1 - \phi^2)$ with two minima occurring at $\phi = 0$ and $\phi = 1$. $g(\phi)$ is a function given by $g(\phi) = 4\phi^3 - 3\phi^4$ and has properties such that $g(0) = 0, g(1) = 1$ and $g'(0) = g'(1) = 0$. With these conditions there always exist two minimas at $\phi = 0$ and $\phi = 1$, and the absolute minimum changes from 1 to 0 as $\bar{\epsilon}^2$ becomes larger than ϵ_c^2 .

τ is the time scale constant which is connected to the relaxation rate of the phase field and D_ϕ is the constant which specifies the width of the interface between the cracked and the uncracked region.

Now computing the variational derivative of energy equation (eq. 3.1) with respect to the displacement gives the second equation,

$$\rho \frac{\partial^2 u}{\partial t^2} + b \frac{\partial u}{\partial t} = \mu \vec{\nabla} \cdot \left[g(\phi) \vec{\nabla} \left(1 + \eta \frac{\partial}{\partial t} \right) u \right] \quad (3.3)$$

where ρ is the mass density, η is the Kelvin viscosity and b is the coefficient of Stokes drag. The term $\partial u / \partial t$ is the Stokes drag term which causes the damping effect in crack growth. η , which is the Kelvin viscosity term, is present in every wave equation which provides a damping effect.

In this study the Kelvin viscosity term is not considered (i.e. $\eta = 0$) and the displacement equation becomes

$$\rho \frac{\partial^2 u}{\partial t^2} + b \frac{\partial u}{\partial t} = \mu \vec{\nabla} \cdot (g(\phi) \vec{\nabla} u) \quad (3.4)$$

To solve this problem of fracture the equations 3.2 and 3.4 are solved simultaneously.

At equilibrium the equations becomes time independent and the time derivatives become zero. Therefore for a one-dimensional case with boundary conditions $u(\pm L) = \pm \delta$ and $\phi(\pm L) = 1$, the strain becomes $\epsilon(y) = \partial_y u = \epsilon_0 / g[\phi(y)]$ and at the boundary strain

becomes, $\epsilon(L) = \epsilon_0$. Therefore at equilibrium eq. 2 becomes,

$$0 = D_\phi \phi'' - W'_{DW}(\phi) - \frac{\mu}{2} g'(\phi) \left(\frac{\epsilon_0^2}{g^2(\phi)} - \epsilon_c^2 \right)$$

Integrating this equation we get,

$$\left(\frac{d\phi}{dy} \right)^2 = E_0 + W_{DW} - \frac{\mu}{2} \left(g(\phi) \epsilon_c^2 + \frac{\epsilon_0^2}{g(\phi)} \right).$$

Assume that effective potential is V_{eff} and is given by,

$$V_{eff} = -W_{DW} + \frac{\mu}{2} \left(g(\phi) \epsilon_c^2 + \frac{\epsilon_0^2}{g(\phi)} \right)$$

and E_0 is a integration constant potential which acts as critical potential. The effective potential profile is shown below

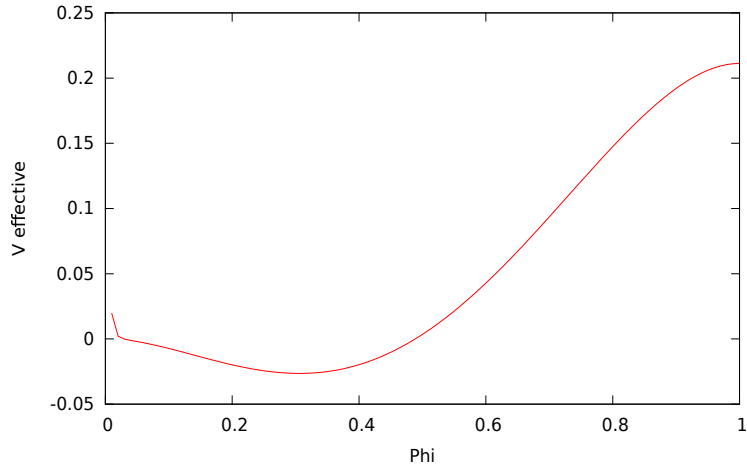


Figure 3.1: Effective potential plot with $\epsilon_c = 0.65$, $\epsilon_0 = 0.0004$ and $\mu = 1.0$

The effective potential have a turning point and that is termed as ϕ^* and this turning point exist near $\phi = 0$ as the for smaller ϕ the $\epsilon_0^2/g(\phi)$ becomes large and at $\phi = 1$ there is local maxima present.

Thus the steady state crack is given by,

$$\frac{1}{\sqrt{2}} \int_{\phi^*}^1 \frac{d\tilde{\phi}}{\sqrt{E_0 - V_{eff}(\tilde{\phi})}} = y$$

and boundary condition fixes the two unknowns ϵ_0 and E_0 and the total integrated strain is given by,

$$\frac{\epsilon_0}{\sqrt{2}} \int_{\phi^*}^1 \frac{d\tilde{\phi}}{g(\tilde{\phi}) \sqrt{E_0 - V_{eff}(\tilde{\phi})}} = \Delta$$

This total integrated strain should scale with \sqrt{L} according to the Griffith condition for fracture. Also the fracture energy is derived in the limit of $\epsilon_0 \rightarrow 0$ and $E_0 \rightarrow \mu\epsilon_c^2/2$ and is given by

$$\gamma = \sqrt{2} \int_0^1 \sqrt{\mu\epsilon_c^2/2 - V_{eff}(\tilde{\phi}; \epsilon_0 = 0)} d\tilde{\phi}$$

According to Griffith theory of fracture, there must be a critical stress or strain for every system. This critical strain for the present model provides a critical displacement which is given by $\Delta_c = \sqrt{2\gamma L}$ and crack propagation starts only when the this Griffith threshold is crossed (i.e. for $\Delta > \Delta_c$).

3.2 Anisotropic Shear Modulus

Now to introduce anisotropy into the present model, the shear modulus of the domain is made anisotropic. As the elastic constant is related to the surface energy, therefore as shear modulus becomes anisotropic the surface energy also becomes anisotropic. And as the surface energy becomes anisotropic the crack will tend to propagate through a path which causes the creation of surface having the least surface energy to minimize the total energy of the system. The mathematical model for this anisotropic case is described below.

Shear Modulus of the system is made anisotropic using the following modification,

$$\mu = \mu_0 a_c^2(\theta)$$

where a_c is the anisotropic function and is given as,

$$a_c = (1 + \delta_{\alpha\beta} \cos 4\theta)$$

$$\theta = \tan^{-1}\left(\frac{n_x}{n_y}\right)$$

where, $n_y = \cos\theta$ and $n_x = \sin\theta$

The polar plot of this anisotropic shear modulus is shown below.

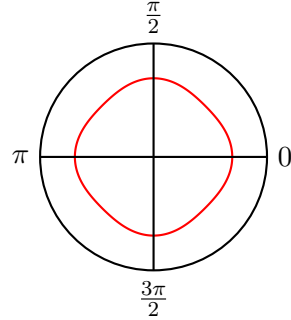


Figure 3.2: Polar plot of anisotropic Shear Modulus.

Here $\delta_{\alpha\beta}$ represents the strength of the anisotropy. The anisotropic function is written in such a way that the maximum and minimum value of shear modulus is related as shown below,

$$\mu_{max} - \mu_{min} = 4\delta_{\alpha\beta}\mu_0$$

$$\mu_{(\theta=0^0)} - \mu_{(\theta=45^0)} = 4\delta_{\alpha\beta}\mu_0$$

By using this anisotropic shear modulus the surface energy of the system is indirectly changed and also the mobility of the system is changed in such a way that the crack will tend to propagate where the surface energy is minimum.

We know that,

$$(cos4\theta + i sin4\theta) = (cos\theta + i sin\theta)^4$$

Now considering only the real part, and expanding the above equation, we get

$$cos4\theta = cos^4\theta + sin^4\theta - 6cos^2\theta sin^2\theta$$

$$cos4\theta = n_x^4 + n_y^4 - 6n_x^2 n_y^2$$

and $n_x^2 + n_y^2 = 1$

$$\therefore (n_x^2 + n_y^2)^2 = 1$$

$$n_x^4 + n_y^4 + 2n_x^2 n_y^2 = 1$$

$$\therefore n_x^2 n_y^2 = \frac{1 - n_x^4 - n_y^4}{2}$$

Substituting the value of $(n_x^2 n_y^2)$ in $\cos 4\theta$, we get,

$$\begin{aligned}\cos 4\theta &= n_x^4 + n_y^4 - 6 \frac{(1 - n_x^4 - n_y^4)}{2} \\ \cos 4\theta &= 4(n_x^4 + n_y^4) - 3\end{aligned}$$

Now substituting the value of $\cos 4\theta$ back in a_c , we get,

$$\begin{aligned}a_c &= 1 + \delta_{\alpha\beta}(4(n_x^4 + n_y^4) - 3) \\ a_c &= 1 - \delta_{\alpha\beta}(3 - 4(n_x^4 + n_y^4)) \\ a_c &= 1 - \delta_{\alpha\beta}\left(3 - 4\left(\frac{\nabla\phi_x^4 + \nabla\phi_y^4}{|\nabla\phi|^4}\right)\right)\end{aligned}$$

where $|\nabla\phi| = \sqrt{\nabla\phi_x^2 + \nabla\phi_y^2}$.

The contribution of this anisotropy to the energy of the system is given by the following term,

$$\begin{aligned}f &= \frac{1}{2}\mu(\epsilon^2 - \epsilon_c^2)g(\phi) \\ f &= \frac{1}{2}\mu_0 a_c^2(n)(\epsilon^2 - \epsilon_c^2)g(\phi)\end{aligned}$$

The dynamics of this anisotropy is calculated by,

$$\partial_t\phi = -\frac{\delta f}{\delta\phi}$$

where,

$$\frac{\delta f}{\delta\phi} = \left(\frac{\delta}{\delta\phi} - \nabla \cdot \frac{\delta}{\delta\nabla\phi}\right)f$$

therefore,

$$\partial_t\phi = -\frac{1}{2}\mu_0 a_c^2(n)(\epsilon^2 - \epsilon_c^2)g'(\phi) + \frac{1}{2}\mu_0(\epsilon^2 - \epsilon_c^2)g(\phi)\nabla_i\left[\frac{\partial}{\partial\nabla\phi}a_c^2(n)\right]$$

where,

$$\begin{aligned}\nabla_i\left[\frac{\partial}{\partial\nabla\phi}a_c^2(n)\right] &= \begin{pmatrix} \frac{\partial}{\partial\nabla\phi_x} \\ \frac{\partial}{\partial\nabla\phi_y} \end{pmatrix} a_c^2 \\ &= 2a_c \begin{pmatrix} \frac{\partial}{\partial\nabla\phi_x} \\ \frac{\partial}{\partial\nabla\phi_y} \end{pmatrix} a_c\end{aligned}$$

and,

$$\begin{aligned}\frac{\partial a_c}{\partial \nabla \phi_x} &= 4\delta_{\alpha\beta} \left(\frac{4\nabla \phi_x^3}{(\nabla \phi_x^2 + \nabla \phi_y^2)^2} + \frac{(-2)(2\nabla \phi_x)(\nabla \phi_x^4 + \nabla \phi_y^4)}{(\nabla \phi_x^2 + \nabla \phi_y^2)^3} \right) \\ &= 16\delta_{\alpha\beta} \left(\frac{\nabla \phi_x^3(\nabla \phi_x^2 + \nabla \phi_y^2) - \nabla \phi_x(\nabla \phi_x^4 + \nabla \phi_y^4)}{(\nabla \phi_x^2 + \nabla \phi_y^2)^3} \right)\end{aligned}$$

Similarly,

$$\frac{\partial a_c}{\partial \nabla \phi_y} = 16\delta_{\alpha\beta} \left(\frac{\nabla \phi_y^3(\nabla \phi_x^2 + \nabla \phi_y^2) - \nabla \phi_y(\nabla \phi_x^4 + \nabla \phi_y^4)}{(\nabla \phi_x^2 + \nabla \phi_y^2)^3} \right)$$

therefore,

$$\nabla_i \left[\frac{\partial}{\partial \nabla \phi} a_c^2(n) \right] = 32\delta_{\alpha\beta} a_c \begin{bmatrix} \frac{\nabla \phi_x^3(\nabla \phi_x^2 + \nabla \phi_y^2) - \nabla \phi_x(\nabla \phi_x^4 + \nabla \phi_y^4)}{(\nabla \phi_x^2 + \nabla \phi_y^2)^3} \\ \frac{\nabla \phi_y^3(\nabla \phi_x^2 + \nabla \phi_y^2) - \nabla \phi_y(\nabla \phi_x^4 + \nabla \phi_y^4)}{(\nabla \phi_x^2 + \nabla \phi_y^2)^3} \end{bmatrix}$$

let

$$\begin{aligned}aniso_x &= \frac{\nabla \phi_x^3(\nabla \phi_x^2 + \nabla \phi_y^2) - \nabla \phi_x(\nabla \phi_x^4 + \nabla \phi_y^4)}{(\nabla \phi_x^2 + \nabla \phi_y^2)^3} \\ \text{and } aniso_y &= \frac{\nabla \phi_y^3(\nabla \phi_x^2 + \nabla \phi_y^2) - \nabla \phi_y(\nabla \phi_x^4 + \nabla \phi_y^4)}{(\nabla \phi_x^2 + \nabla \phi_y^2)^3}\end{aligned}$$

therefore,

$$\nabla_i \left[\frac{\partial}{\partial \nabla \phi} a_c^2(n) \right] = 32\delta_{\alpha\beta} \nabla \cdot \left(a_c \begin{bmatrix} aniso_x \\ aniso_y \end{bmatrix} \right)$$

and now the evolution equation becomes,

$$\partial_t \phi = -\frac{1}{2} \mu_0 a_c^2(n) (\epsilon^2 - \epsilon_c^2) g'(\phi) + 16\delta_{\alpha\beta} \mu_0 (\epsilon^2 - \epsilon_c^2) g(\phi) \nabla \cdot \left(a_c \begin{bmatrix} aniso_x \\ aniso_y \end{bmatrix} \right)$$

Now in order to solve this anisotropy problem, the above evolution equation is solved simultaneously with the displacement evolution equation (equation 3.4).

3.3 Multi Grains

In this particular section, crack propagation is studied for a material containing multiple grains. Each grain is assumed to be a different phase having different shear modulus. Shown below is the grained structure of the material.

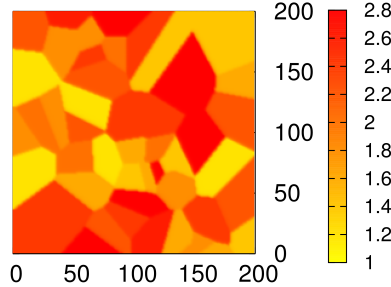


Figure 3.3: Grained structure of the material.

The above figure shows different grains represented by different color. The grain with darker shade has larger shear modulus and the grain with lighter shade has lower shear modulus. As the color changes from dark red to yellow, the shear modulus decreases.

Now to simulate different grains in the material Voronoi tessellation [9] is used. To distinguish different grains from one another a different phase field variable η is defined, such that for i^{th} grain η_i takes the value of 1.0 and other η 's take the value of 0.0. And in the grain boundary between the grains i and j , η_i and η_j take a value between 0.0 and 1.0, such that $\eta_i + \eta_j = 1.0$ and all other η are zero.

Now to distinguish grains from one another, different shear modulus (μ) values are assigned to different grains. This causes the effective shear modulus at any given grid point to become as follows,

$$\mu = \sum_{i=0}^n \mu_i h(\eta_i)$$

where $h(\eta_i)$ is a function represented as, $h(\eta_i) = \eta_i$.

Now the governing equation for the present case becomes,

$$\begin{aligned} \tau \partial_t \phi &= D_\phi \nabla^2 \phi - W'_{WD}(\phi) - \frac{\mu}{2} g'(\phi) (\bar{\epsilon}^2 - \epsilon_c^2) \\ \rho \frac{\partial^2 u}{\partial t^2} + b \frac{\partial u}{\partial t} &= \vec{\nabla} \cdot [\mu g(\phi) \vec{\nabla} u] \end{aligned}$$

To solve this multi-grain problem, the above two governing equations are simultaneously solved.

Chapter 4

Solving Techniques

The present phase field problem can be solved using two different numerical methods,

- Explicit Method
- Implicit Method

Both these schemes are used to solve the numerical problem involving time dependent ordinary and partial differential equations.

4.1 Explicit Scheme

In the explicit scheme the dependent variable can be easily represented in term of the known quantities, and direct iterative method can be used to solve the time dependent problem. The explicit scheme has a tendency to remain stable only when the time step (dt) used is sufficiently small. However the explicit method are simple to implement. But as the time step required decreases, the computational time goes up.

The present model is discretized for the explicit scheme as follows.

4.1.1 Discretization of the Model

The ϕ equation (eq. 3.2) is discretized using the simple forward difference method. The discretized equation is

$$\begin{aligned}\tau \partial_t \phi(\vec{x}, t) &= D_\phi \nabla^2 \phi - W'_{DW}(\phi) - \frac{\mu}{2} g'(\phi)(\bar{\epsilon}^2 - \epsilon_c^2) \\ \tau \frac{(\phi_{i,j}^{t+1} - \phi_{i,j}^t)}{dt} &= D_\phi \left(\frac{\frac{(\phi_{i+1,j}^t - \phi_{i,j}^t)}{dx} - \frac{(\phi_{i,j}^t - \phi_{i-1,j}^t)}{dx}}{dx} + \frac{\frac{(\phi_{i,j+1}^t - \phi_{i,j}^t)}{dy} - \frac{(\phi_{i,j}^t - \phi_{i,j-1}^t)}{dy}}{dy} \right) \\ &\quad - W'_{DW}(\phi) - \frac{\mu}{2} g'(\phi)(\bar{\epsilon}^2 - \epsilon_c^2)\end{aligned}$$

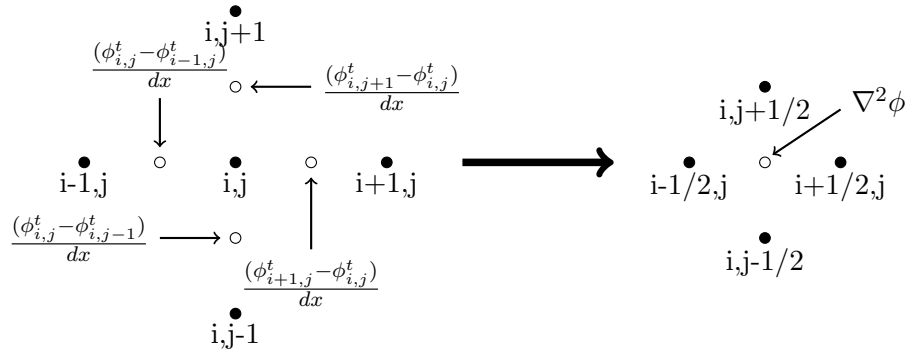


Figure 4.1: Discretization of the domain for calculating the Laplacian of ϕ .

The laplacian of ϕ ($\nabla^2 \phi$) is calculated as shown in Figure 4.1, and W'_{DW} , $g'(\phi)$ and ϵ are calculated as shown below,

$$\begin{aligned}W_{DW} &= \frac{1}{4} \phi^2 (1 - \phi)^2 \\ \therefore W'_{DW} &= \frac{1}{2} \phi (1 - \phi) (1 - 2\phi) \\ g(\phi) &= 4\phi^3 - 3\phi^4 \\ \therefore g'(\phi) &= 12\phi^2 (1 - \phi) \\ \epsilon &= \nabla u \\ \therefore \epsilon &= \frac{u_{i+1,j}^t - u_{i-1,j}^t}{2dx} + \frac{u_{i,j+1}^t - u_{i,j-1}^t}{2dy} \\ \therefore |\epsilon| &= \sqrt{\left(\frac{u_{i+1,j}^t - u_{i-1,j}^t}{2dx} \right)^2 + \left(\frac{u_{i,j+1}^t - u_{i,j-1}^t}{2dy} \right)^2}\end{aligned}$$

the magnitude of the gradient of displacement is used in the strain calculation and the discretization is done by central difference as shown in Figure 4.2 below;

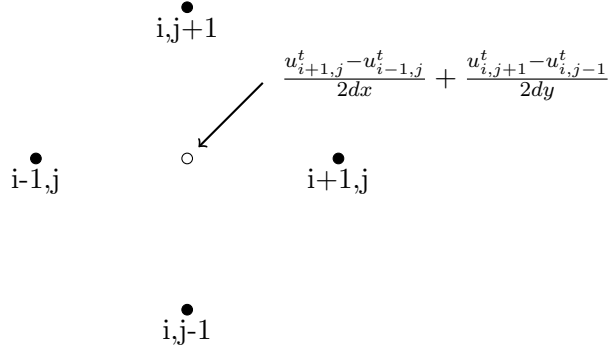


Figure 4.2: Discretization of domain for calculating the gradient of u .

The evolution of the displacement equation is done by making a simple assumption that,

$$\frac{\partial u}{\partial t} = v$$

therefore the displacement equation becomes

$$\rho \frac{\partial v}{\partial t} + bv = \mu \vec{\nabla} \cdot (g(\phi) \vec{\nabla} u)$$

Now the discretization of this equation is done using simple forward difference method as shown follows,

$$\begin{aligned} \rho \frac{\partial v}{\partial t} + bv &= \mu \vec{\nabla} \cdot (g(\phi) \vec{\nabla} u) \\ \rho \frac{\partial v}{\partial t} + bv &= \mu \vec{\nabla} \cdot \left(g(\phi) \left[\begin{array}{c} \frac{\partial u}{\partial x} \\ \frac{\partial u}{\partial y} \end{array} \right] \right) \\ \rho \frac{\partial v}{\partial t} + bv &= \mu \vec{\nabla} \cdot \left(g(\phi)_{i,j}^t \left[\begin{array}{c} \frac{u_{i+1,j}^t - u_{i,j}^t}{\Delta x} \\ \frac{u_{i,j+1}^t - u_{i,j}^t}{\Delta y} \end{array} \right] \right) \end{aligned}$$

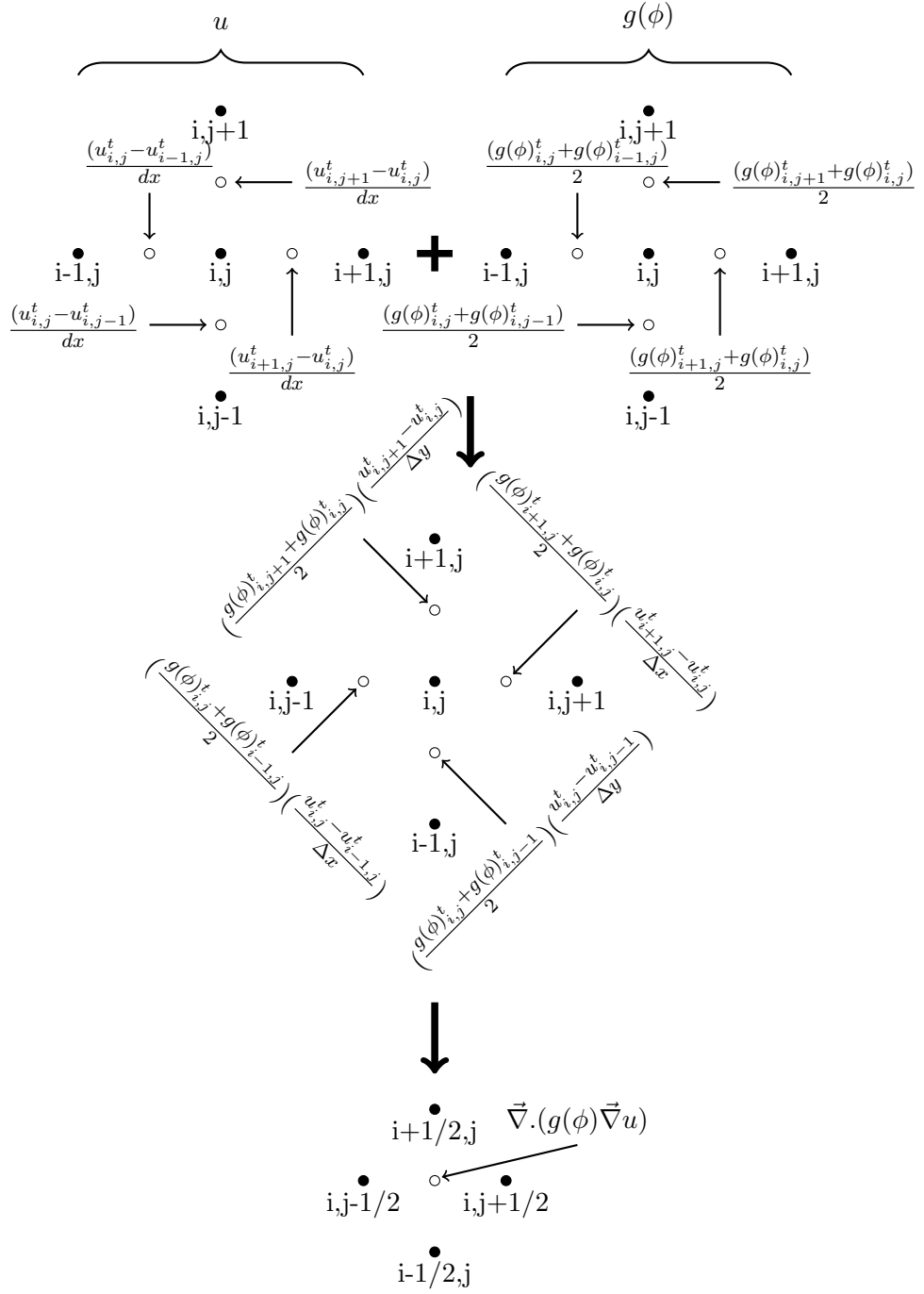


Figure 4.3: Discretization of the domain, first distretizing domain for the displacement and then for $g(\phi)$ to finally find $\vec{\nabla} \cdot (g(\phi) \vec{\nabla} u)$

$$\begin{aligned} \rho \frac{\partial v}{\partial t} + bv &= \mu \left(\frac{\left(\frac{g(\phi)_{i+1,j}^t + g(\phi)_{i,j}^t}{2}\right)\left(\frac{u_{i+1,j}^t - u_{i,j}^t}{\Delta x}\right) - \left(\frac{g(\phi)_{i,j}^t + g(\phi)_{i-1,j}^t}{2}\right)\left(\frac{u_{i,j}^t - u_{i-1,j}^t}{\Delta x}\right)}{\Delta x} \right. \\ &\quad \left. + \frac{\left(\frac{g(\phi)_{i,j+1}^t + g(\phi)_{i,j}^t}{2}\right)\left(\frac{u_{i,j+1}^t - u_{i,j}^t}{\Delta y}\right) - \left(\frac{g(\phi)_{i,j}^t + g(\phi)_{i,j-1}^t}{2}\right)\left(\frac{u_{i,j}^t - u_{i,j-1}^t}{\Delta y}\right)}{\Delta y} \right) \\ \rho \frac{(v_{i,j}^{t+1} - v_{i,j}^t)}{\Delta t} + bv_{i,j}^t &= \mu \left(\frac{\left(\frac{g(\phi)_{i+1,j}^t + g(\phi)_{i,j}^t}{2}\right)\left(\frac{u_{i+1,j}^t - u_{i,j}^t}{\Delta x}\right) - \left(\frac{g(\phi)_{i,j}^t + g(\phi)_{i-1,j}^t}{2}\right)\left(\frac{u_{i,j}^t - u_{i-1,j}^t}{\Delta x}\right)}{\Delta x} \right. \\ &\quad \left. + \frac{\left(\frac{g(\phi)_{i,j+1}^t + g(\phi)_{i,j}^t}{2}\right)\left(\frac{u_{i,j+1}^t - u_{i,j}^t}{\Delta y}\right) - \left(\frac{g(\phi)_{i,j}^t + g(\phi)_{i,j-1}^t}{2}\right)\left(\frac{u_{i,j}^t - u_{i,j-1}^t}{\Delta y}\right)}{\Delta y} \right) \end{aligned}$$

The pictorial discretization of the above displacement equation is shown in Figure 4.3.

4.1.1.1 Boundary Conditions

For the phase profile the boundary condition used is Neumann boundary condition in both x and y directions.

$$\begin{array}{ll} \text{for y-direction} & \phi_{i,j}^{t+1} = \phi_{i+1,j}^{t+1} \\ \text{for x-direction} & \phi_{i,j}^{t+1} = \phi_{i,j+1}^{t+1} \end{array}$$

And for the displacement profile the boundary condition used in the side boundaries is Neumann boundary condition and for the top and bottom boundary constant or Dirichlet boundary condition is used.

$$\begin{array}{ll} \text{for x-direction} & u_{i,j}^{t+1} = u_{i,j+1}^{t+1} \\ \text{for y-direction} & u_{i,j}^{t+1} = u_{i,j}^t \end{array}$$

These boundary conditions are applied separately at the end of each time step.

4.1.2 Discretization of the Anisotropic Model

4.1.2.1 To calculate $a_c^2(n)$

Both $\nabla\phi_x$ and $\nabla\phi_y$ are calculated using central difference method.

$$\nabla\phi_{x,i,j} = \frac{\phi_{i+1,j} - \phi_{i-1,j}}{2dx}$$

and

$$\nabla\phi_{y,i,j} = \frac{\phi_{i,j+1} - \phi_{i,j-1}}{2dy}$$

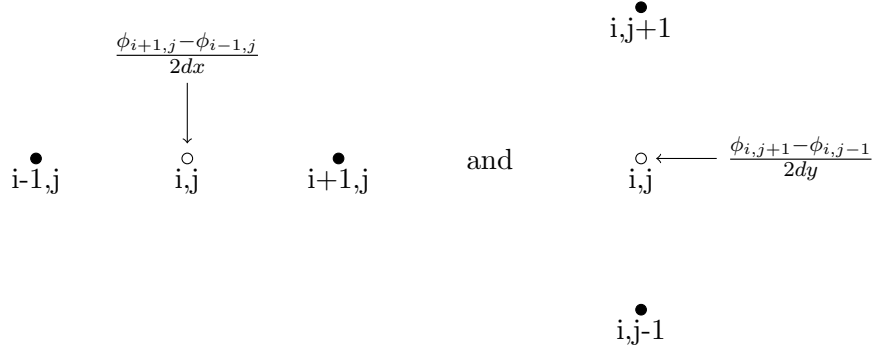


Figure 4.4: Discretization to calculate $\nabla\phi_x$ and $\nabla\phi_y$ using central difference method.

4.1.2.2 To calculate $\nabla_i \left[\frac{\partial}{\partial \nabla \phi} a_c^2(n) \right]$

$$\nabla_i \left[\frac{\partial}{\partial \nabla \phi} a_c^2(n) \right] = 32\delta_{\alpha\beta} \nabla \cdot \left(a_c \begin{bmatrix} aniso_x \\ aniso_y \end{bmatrix} \right)$$

To discretize the matrix for the above equation, we have to discretize the $aniso_x$ and $aniso_y$ first. They are discretized using forward difference method.

4.1.2.3 Discretization of $aniso_x$

First $\nabla\phi_x$ is calculated using backward difference method.

$$\nabla\phi_{x,i,j} = \frac{\phi_{i,j} - \phi_{i-1,j}}{dx}$$

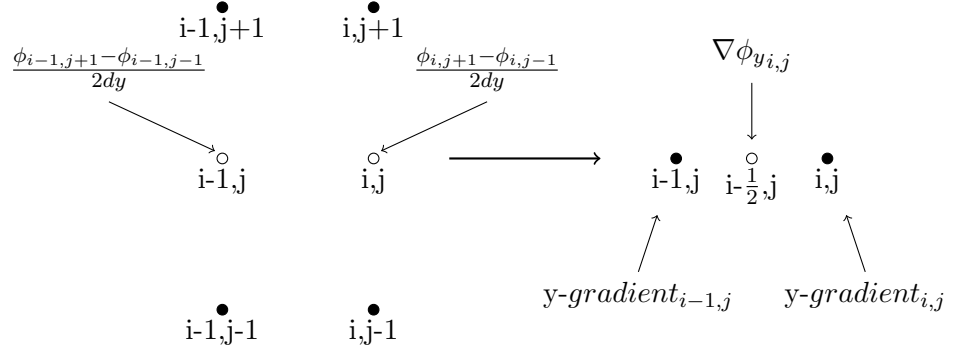
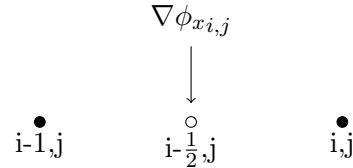
Then $\nabla\phi_y$ is calculated by taking the average of the y-gradient of ϕ calculate using central difference method at (i, j) and $(i - 1, j)$, so that $\nabla\phi_y$ is calculated at the same point $\nabla\phi_x$ is calculated above, i.e. $(i - 1/2, j)$.

$$y - gradient_{i,j} = \frac{\phi_{i,j+1} - \phi_{i,j-1}}{2dy}$$

$$y - gradient_{i-1,j} = \frac{\phi_{i-1,j+1} - \phi_{i-1,j-1}}{2dy}$$

and

$$\nabla\phi_{y,i,j} = \frac{y - gradient_{i,j} + y - gradient_{i-1,j}}{2}$$

**Figure 4.5:** Discretization of matrix to calculate $\nabla\phi_y$ for $aniso_x$.**Figure 4.6:** Discretization of matrix to calculate $\nabla\phi_x$ for $aniso_x$.

4.1.2.4 Discretization of $aniso_y$

Similarly first $\nabla\phi_y$ is calculated using backward difference method.

$$\nabla\phi_{x,i,j} = \frac{\phi_{i,j} - \phi_{i,j-1}}{dy}$$

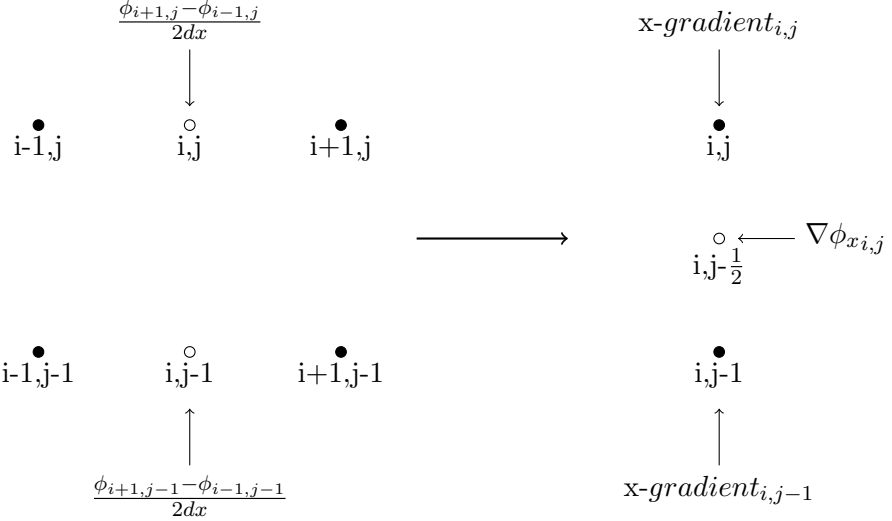
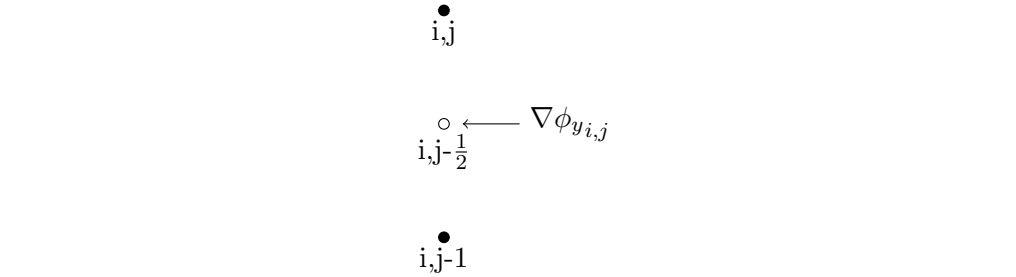
Then $\nabla\phi_x$ is calculated by taking the average of the x-gradient of ϕ calculate using central difference method at (i, j) and $(i, j - 1)$, so that $\nabla\phi_x$ is calculated at the same point $\nabla\phi_y$ is calculated above, i.e. $(i, j - 1/2)$.

$$x - gradient_{i,j} = \frac{\phi_{i+1,j} - \phi_{i-1,j}}{2dx}$$

$$x - gradient_{i,j-1} = \frac{\phi_{i+1,j-1} - \phi_{i-1,j-1}}{2dx}$$

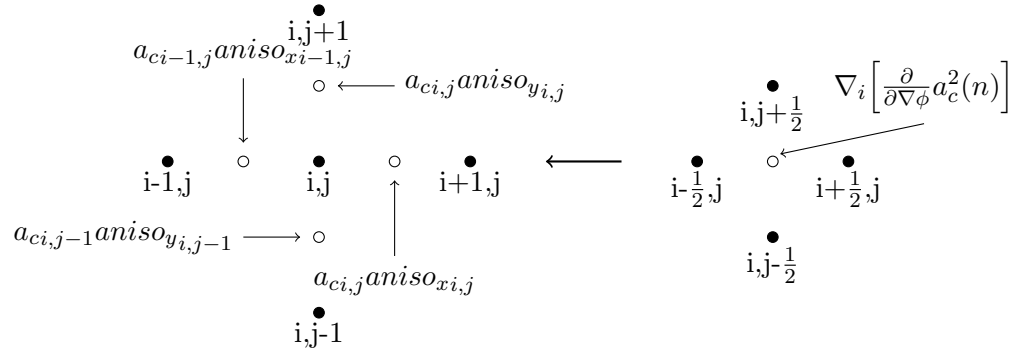
and

$$\nabla\phi_{y,i,j} = \frac{x - gradient_{i,j} + x - gridient_{i,j-1}}{2}$$

**Figure 4.7:** Discretization of matrix to calculate $\nabla\phi_x$ for $aniso_y$.**Figure 4.8:** Discretization of matrix to calculate $\nabla\phi_y$ for $aniso_y$.

Now the final discretized model is done by,

$$\nabla_i \left[\frac{\partial}{\partial \nabla \phi} a_c^2(n)_{i,j} \right] = \frac{a_{ci,j} aniso_{xi,j} - a_{ci-1,j} aniso_{xi-1,j}}{dx} + \frac{a_{ci,j} aniso_{yi,j} - a_{ci,j-1} aniso_{yi,j-1}}{dy}$$

**Figure 4.9:** Discretization of the matrix for the anisotropy term.

4.1.2.5 Boundary Conditions

For the phase profile the boundary condition used is Neumann boundary condition in all four sides of the domain.

For the displacement profile constant boundary condition is used at the top and bottom ends of the domain where stresses are applied and Neumann boundary condition is used at the left and right ends of the domain.

4.1.3 Discretization of Multi Grain Model

The phase field equation of this Multi Grain model is discretized in the same way as the earlier conditions.

The displacement equation is discretized as shown below,

$$\begin{aligned}\frac{\partial u}{\partial t} &= v \\ \rho \frac{\partial v}{\partial t} + bv &= \vec{\nabla} \cdot [\mu g(\phi) \vec{\nabla} u]\end{aligned}$$

Now the equation is discretized using forward difference method as shown below,

$$\rho \frac{v_{i,j}^{t+1} - v_{i,j}^t}{dt} + bv_{i,j}^t = \vec{\nabla} \cdot \left[\begin{array}{c} \left(\frac{\mu_{i+1,j}g(\phi_{i+1,j}^t) + \mu_{i,j}g(\phi_{i,j}^t)}{2} \right) \left(\frac{u_{i+1,j}^t - u_{i,j}^t}{dx} \right) \\ \left(\frac{\mu_{i,j+1}g(\phi_{i,j+1}^t) + \mu_{i,j}g(\phi_{i,j}^t)}{2} \right) \left(\frac{u_{i,j+1}^t - u_{i,j}^t}{dy} \right) \end{array} \right]$$

$$\begin{aligned}\rho \frac{v_{i,j}^{t+1} - v_{i,j}^t}{dt} + bv_{i,j}^t &= \left[\frac{\left(\frac{\mu_{i+1,j}g(\phi_{i+1,j}^t) + \mu_{i,j}g(\phi_{i,j}^t)}{2} \right) \left(\frac{u_{i+1,j}^t - u_{i,j}^t}{dx} \right) - \left(\frac{\mu_{i,j}g(\phi_{i,j}^t) + \mu_{i-1,j}g(\phi_{i-1,j}^t)}{2} \right) \left(\frac{u_{i,j}^t - u_{i-1,j}^t}{dx} \right)}{dx} \right. \\ &\quad \left. + \frac{\left(\frac{\mu_{i,j+1}g(\phi_{i,j+1}^t) + \mu_{i,j}g(\phi_{i,j}^t)}{2} \right) \left(\frac{u_{i,j+1}^t - u_{i,j}^t}{dy} \right) - \left(\frac{\mu_{i,j}g(\phi_{i,j}^t) + \mu_{i,j-1}g(\phi_{i,j-1}^t)}{2} \right) \left(\frac{u_{i,j}^t - u_{i,j-1}^t}{dy} \right)}{dy} \right]\end{aligned}$$

The figure below describes the above discretization,

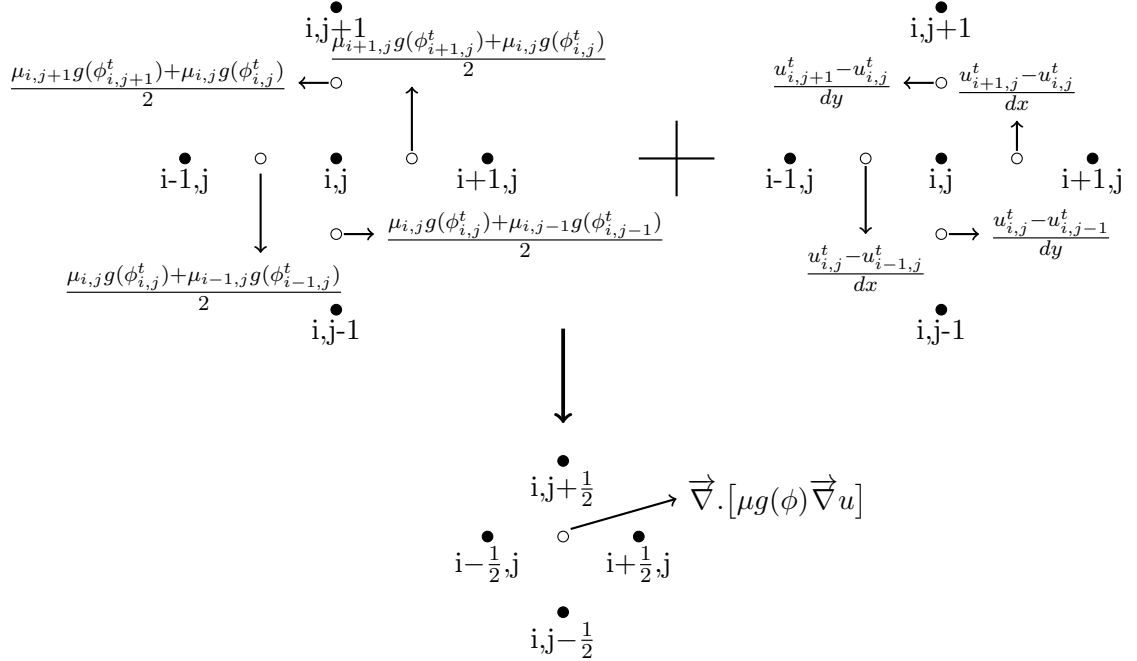


Figure 4.10: Discretization of the domain for solving the displacement field.

4.1.3.1 Boundary Conditions

For the phase profile the boundary condition used is Neumann boundary condition in all four sides of the domain.

For the displacement profile constant boundary condition is used at the top and bottom ends of the domain where stresses are applied and Neumann boundary condition is used at the left and right ends of the domain.

4.2 Implicit Scheme

In the implicit scheme the dependent variables are represented in terms of the known quantities as well as the unknown quantities. The implicit methods find a solution by solving an equation involving both the current state of system as well as the later state of system. The implicit method is unconditionally stable as it is stable for very large values of time step (dt). As the dependent variables are defined by coupled set of equations, a matrix or iterative technique is needed to solve the problem. This makes the implicit scheme computationally expensive but can achieve the solution in less computational time.

The ϕ equation is solved using the same discretization method used for the explicit scheme. To solve the displacement equation a different technique is used.

4.2.1 Douglas Scheme

In this method the system of equations are converted into a set of equations which can be easily written in the form of a tri-diagonal matrix. The scheme involves breaking down the equations into two half step and solving the equations in two parts. This scheme is similar to the Alternating Direction Implicit (ADI) method [8].

Now to solve this double derivative of displacement with time, Douglas Scheme is used along with the Thomas method to solve the tridiagonal system of equations.

First we assume that,

$$\frac{\partial u}{\partial t} = v$$

Therefore, the eq. 3.4 becomes,

$$\rho \frac{\partial v}{\partial t} + bv = \mu \vec{\nabla} \cdot (g(\phi) \vec{\nabla} u)$$

Now lets define two operators Op_x and Op_y such that eq. 4 becomes,

$$\rho \frac{\partial v}{\partial t} + bv = \mu(Op_x + Op_y)u$$

where,

$$Op_x(u_{i,j}^t) = \frac{1}{2\Delta x^2} \left((g(\phi)_{i+1,j}^t + g(\phi)_{i,j}^t)u_{i+1,j}^t - ((g(\phi)_{i+1,j}^t + g(\phi)_{i,j}^t) + (g(\phi)_{i,j}^t + g(\phi)_{i-1,j}^t))u_{i,j}^t + (g(\phi)_{i,j}^t + g(\phi)_{i-1,j}^t)u_{i-1,j}^t \right)$$

and

$$Op_y(u_{i,j}^t) = \frac{1}{2\Delta y^2} \left((g(\phi)_{i,j+1}^t + g(\phi)_{i,j}^t)u_{i,j+1}^t - ((g(\phi)_{i,j+1}^t + g(\phi)_{i,j}^t) + (g(\phi)_{i,j}^t + g(\phi)_{i,j-1}^t))u_{i,j}^t + (g(\phi)_{i,j}^t + g(\phi)_{i,j-1}^t)u_{i,j-1}^t \right)$$

on solving this equation, it reduces to,

$$(1 - \frac{\mu\Delta t^2}{4\rho}(Op_x + Op_y))v_{i,j}^{t+1} = (1 + \frac{b\Delta t}{\rho} + \frac{\mu\Delta t^2}{4\rho}(Op_x + Op_y))v_{i,j}^t + \frac{\mu\Delta t}{\rho}(Op_x + Op_y)u_{i,j}^t$$

Therefor according to the Douglas Scheme,

After half time step,

$$(1 - \frac{\mu\Delta t^2}{4\rho} Op_x)(v_{i,j}^{t+1/2} - v_{i,j}^t) = \left(\frac{b\Delta t}{\rho} + \frac{\mu\Delta t^2}{2\rho}(Op_x + Op_y) \right) v_{i,j}^t + \frac{\mu\Delta t}{\rho}(Op_x + Op_y) u_{i,j}^t \quad (4.1)$$

and at the next half time step,

$$(1 - \frac{\mu\Delta t^2}{4\rho} Op_y)(v_{i,j}^{t+1} - v_{i,j}^t) = (v_{i,j}^{t+1/2} - v_{i,j}^t) \quad (4.2)$$

4.2.2 Thomas Tridiagonal Method

In this method the tridiagonal system of equations are solve by using the simple Gaussian elimination [8]. This is used to solve a equation in one direction. The system of equations has a form of

$$a_i x_{i-1} + b_i x_i + c_i x_{i+1} = d_i$$

And the system of n equations can be represented in a matrix in the form as shown below,

$$\begin{bmatrix} b_1 & c_1 & & & 0 \\ a_2 & b_2 & c_2 & & \\ & a_3 & b_3 & \ddots & \\ & & \ddots & \ddots & c_{n-1} \\ 0 & & & a_n & b_n \end{bmatrix} \times \begin{bmatrix} x_1 \\ x_2 \\ x_3 \\ \vdots \\ x_n \end{bmatrix} = \begin{bmatrix} d_1 \\ d_2 \\ d_3 \\ \vdots \\ d_n \end{bmatrix}$$

where $a_1 = 0$ and $c_n = 0$

And now the equations from the Douglas scheme are expanded to find the coefficients for the tridiagonal set of equations as shown below,

for eq 4.1

$$(v_{i,j}^{t+1/2} - v_{i,j}^t) = x_{i,j}$$

$$(1 - \frac{\mu\Delta t^2}{4\rho} Op_x)x_{i,j} = \left(\frac{b\Delta t}{\rho} + \frac{\mu\Delta t^2}{2\rho}(Op_x + Op_y) \right) v_{i,j}^t + \frac{\mu\Delta t}{\rho}(Op_x + Op_y) u_{i,j}^t$$

and

$$(1 - \frac{\mu\Delta t^2}{4\rho} Op_x)x_{i,j} = x_{i,j} - (\frac{\mu\Delta t^2}{4\rho})(\frac{1}{2\Delta x^2}) \left((g(\phi)_{i+1,j}^t + g(\phi)_{i,j}^t)x_{i+1,j} \right. \\ \left. - ((g(\phi)_{i+1,j}^t + g(\phi)_{i,j}^t) + (g(\phi)_{i,j}^t + g(\phi)_{i-1,j}^t))x_{i,j} \right. \\ \left. + (g(\phi)_{i,j}^t + g(\phi)_{i-1,j}^t)x_{i-1,j} \right)$$

Therefore the coefficients of the Thomas tridiagonal system are,

$$a = -(\frac{\mu\Delta t^2}{8\rho\Delta x^2})(g(\phi)_{i,j}^t + g(\phi)_{i-1,j}^t) \\ b = (1 + (\frac{\mu\Delta t^2}{8\rho\Delta x^2}))((g(\phi)_{i+1,j}^t + g(\phi)_{i,j}^t) + (g(\phi)_{i,j}^t + g(\phi)_{i-1,j}^t)) \\ c = -(\frac{\mu\Delta t^2}{8\rho\Delta x^2})(g(\phi)_{i+1,j}^t + g(\phi)_{i,j}^t) \\ d = \left(\frac{b\Delta t}{\rho} + \frac{\mu\Delta t^2}{2\rho}(Op_x + Op_y) \right) v_{i,j}^t + \frac{\mu\Delta t}{\rho}(Op_x + Op_y) u_{i,j}^t$$

similarly for eq. 4.2,

$$(v_{i,j}^{t+1} - v_{i,j}^t) = x_{i,j} \\ (1 - \frac{\mu\Delta t^2}{4\rho} Op_y)x_{i,j} = (v_{i,j}^{t+1/2} - v_{i,j}^t) \\ (1 - \frac{\mu\Delta t^2}{4\rho} Op_y)x_{i,j} = x_{i,j} - (\frac{\mu\Delta t^2}{4\rho})(\frac{1}{2\Delta y^2}) \left((g(\phi)_{i,j+1}^t + g(\phi)_{i,j}^t)x_{i,j+1} \right. \\ \left. - ((g(\phi)_{i,j+1}^t + g(\phi)_{i,j}^t) + (g(\phi)_{i,j}^t + g(\phi)_{i,j-1}^t))x_{i,j} \right. \\ \left. + (g(\phi)_{i,j}^t + g(\phi)_{i,j-1}^t)x_{i,j-1} \right)$$

therefore the coefficients of the Thomas tridiagonal system becomes

$$a = -(\frac{\mu\Delta t^2}{8\rho\Delta y^2})(g(\phi)_{i,j}^t + g(\phi)_{i,j-1}^t) \\ b = (1 + (\frac{\mu\Delta t^2}{8\rho\Delta y^2}))((g(\phi)_{i,j+1}^t + g(\phi)_{i,j}^t) + (g(\phi)_{i,j}^t + g(\phi)_{i,j-1}^t)) \\ c = -(\frac{\mu\Delta t^2}{8\rho\Delta y^2})(g(\phi)_{i,j+1}^t + g(\phi)_{i,j}^t) \\ d = (v_{i,j}^{t+1/2} - v_{i,j}^t)$$

The basic algorithm for the Thomas scheme is written below

For a system of n equations, there are $n - 2$ equations to be solved in the tridiagonal

system of equations.

The sub routine for Thomas Algorithm

```

for i = 3 to n-1
do
    b(i) = b(i) - ( a(i) × c(i-1) ) / b(i-1)
    d(i) = d(i) - ( a(i) × d(i-1) ) / b(i-1)
loop
    x(n-1) = d(n-2) / b(n-2)
for i = n-1 to 3 step -1
do
    x(i-1) = ( d(i-1) - c(i-1) × x(i) ) / b(i-1)
loop
```

where $x(1)$ and $x(n)$ are known because of the boundary condition.

4.2.3 Boundary Conditions

For the phase profile the boundary condition applied is Neumann boundary condition for both x and y direction and is applied using same method as in the explicit scheme.

For the displacement profile Neumann boundary condition is applied in x direction and Dirichlet (or constant) boundary condition is applied in the y direction. These boundary conditions are incorporated in the system of equation via Thomas scheme which is used to solve the displacement equation.

Chapter 5

Results and Discussions

5.1 Introduction

The present mathematical model [1] was first verified with the Griffith's theory. The critical value of the applied displacement (Δ_c) was found in this model. Simulations were done to verify the linear dependence of this critical displacement (Δ_c) with the domain length. Stress ahead of the crack tip was calculated and matched with the analytical solution. Crack branching instability was simulated, which is similar to actual cracking scenario. Simulations where crack is propagating through an anisotropic domain were carried out. Crack propagating through a multi-phase domain was simulated. The influence of the multi-phase environment in front of the crack and the distribution of phases in the domain in crack propagation were studied.

All the situations mentioned above were discussed in detail further in this chapter.

5.2 Non-dimensionalization

The mathematical model used for simulating the crack propagation behavior [1] is shown below,

$$\tau \partial_t \phi(\vec{x}, t) = D_\phi \nabla^2 \phi - W'_{DW}(\phi) - \frac{\mu}{2} g'(\phi) (\vec{\epsilon}^2 - \epsilon_c^2)$$

and

$$\rho \frac{\partial^2 u}{\partial t^2} + b \frac{\partial u}{\partial t} = \mu \vec{\nabla} \cdot [g(\phi) \vec{\nabla} u]$$

Both the above equations are non-dimensionalised. In this above mentioned model, $\sqrt{D_\phi}$ represents the characteristics length scale, the interface width. τ represents the time for relaxation of the phase field and there is an another time scale which is related to the relaxation time of the strain or stress field in the model. The τ selected for the model is such that the phase field relax much faster than the strain or stress field so that the equations become strain controlled.

In this model $\sqrt{\frac{\mu}{\rho}}$ represents the speed of sound which is the maximum possible crack propagation velocity in this model. The characteristics time scale (t^*) in this model is given by,

$$t^* = \frac{\sqrt{D_\phi}}{\sqrt{\mu/\rho}}$$

The time conversion in this model is given as ,

$$t = t^* \Delta t$$

where Δt is the total time steps in the simulation.

There is a energy scale in this model which is given by μ .

5.3 Critical Delta

Initially the fracture energy is calculated using given equation [1],

$$\gamma = \sqrt{2} \int_0^1 \sqrt{\mu \epsilon_c^2 / 2 - V_{eff}(\tilde{\phi}; \epsilon_0 = 0)} d\tilde{\phi}$$

Hear the ϵ_c (i.e. the critical strain) is considered to be 0.65 which is kept constant throughout the calculation. And with μ kept at 1.0, the fracture energy calculated is 0.3464.

And using this fracture energy the critical delta at equilibrium was found to be 3.722.

Therefore at any higher delta the crack should propagate and this is also observed in the simulations. The velocity of crack propagation is calculated with decreasing delta and a critical delta is found out at which the crack is at equilibrium.

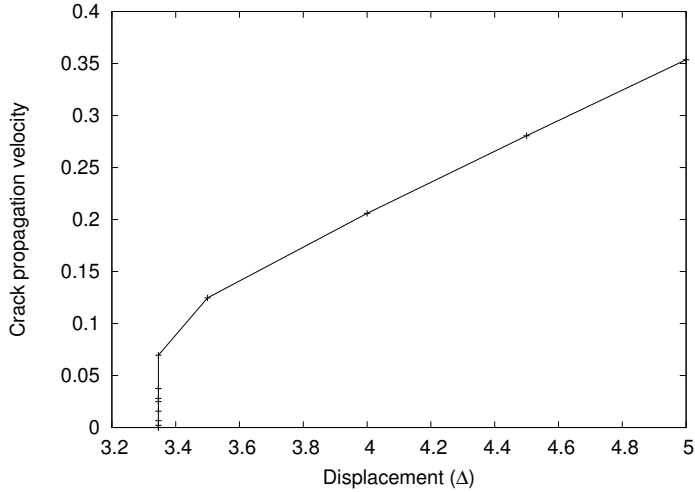


Figure 5.1: Change in velocity with delta giving an equilibrium point.

The above figure is calculated by calculating the crack propagation velocity for different applied displacement (Δ). It can be seen that the crack velocity is decreasing with decreasing Δ and at a certain Δ the crack velocity is becoming zero and beyond this point the crack is not propagating. This particular displacement is said to be critical displacement (Δ_c) and it shows that Griffith point exists in the present simulation.

The critical displacement (Δ_c) was found out to be 3.3459, which is close to what the expected value obtained earlier from the fracture energy calculation.

The following shows the simulated results at different Δ 's and it replicate the Griffith's theory. Figure 5.2 shows that the crack is growing when the applied Δ is larger than the equilibrium Δ . And similarly the Figure 5.3 shows that the crack is shrinking when the applied Δ is smaller than the equilibrium value. This is an artifact of the phase field model, where the process is reversible and hence the crack closure can occur. The color red indicates the crack and the color blue indicates the matrix and the color green indicates the exact interface between crack and the matrix.

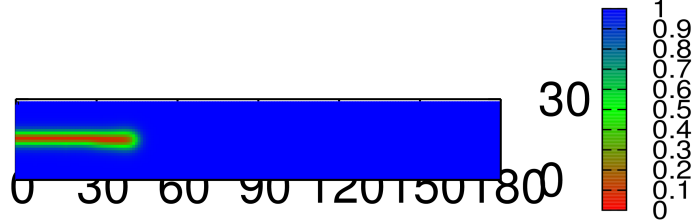


Figure 5.2: Crack growing above the critical delta ($\Delta = 4$).

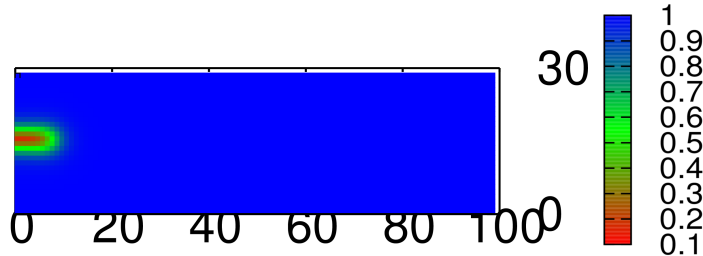


Figure 5.3: Crack shrinking below the critical delta ($\Delta = 3.345$).

The steady state propagation of crack can be interpreted with the help of velocity profile of crack. The crack velocity is obtained by monitoring the crack interface at the crack tip. The exact interface is assumed to be located at the point where $\phi = 0.5$.

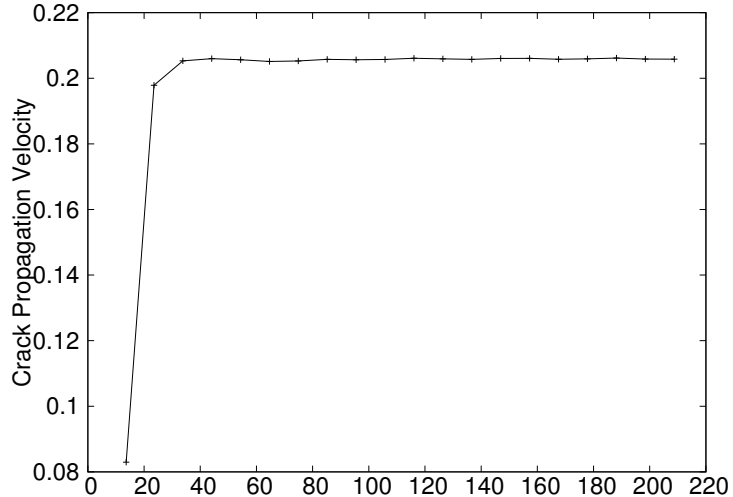


Figure 5.4: Velocity of crack propagation at delta = 4.

From the Figure 5.4 it can be seen that the crack is propagating at a constant velocity, and hence the simulation is producing a steady state crack growth. Analytically velocity of crack propagation cannot be obtained from the usual continuum theory without additional assumptions[1].

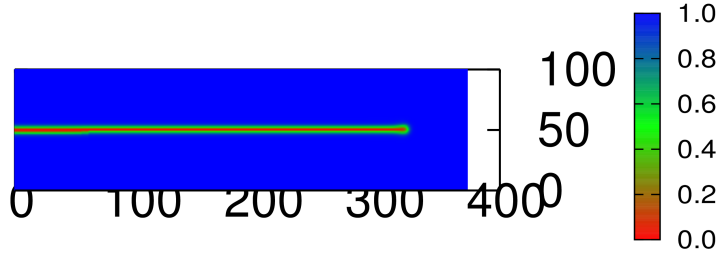


Figure 5.5: Steady state crack propagation.

The Figure 5.5 shows a crack propagation having the velocity profile shown in Figure 5.4. From these figures it can be seen that the present model is able to simulate a steady state crack propagation. Here the simulation is carried out in a infinitely long matrix. The color red indicates the crack and blue indicates the matrix with the interface is indicated by the green color. The other colors indicate the interface between the phases.

5.4 Comparison with Griffith's Model

According to Griffith's model for brittle material [7], the critical stress above which the crack propagation starts is given as

$$\sigma_c = \left(\frac{2E'\gamma}{\pi a_c} \right)^{1/2}$$

For a mode III crack propagation the stress applied is a shear stress and is given as,

$$\tau_c = \sigma_c = 2E' \epsilon_c$$

where μ is the shear modulus and ϵ_c is the critical shear strain.

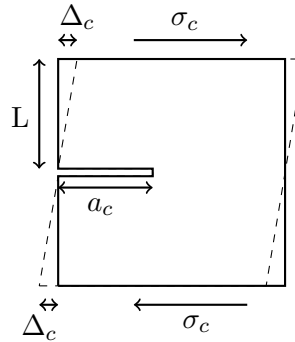


Figure 5.6: Shear stress applied to a sample containing crack.

The critical shear strain in this case can be written as,

$$\epsilon_c = \frac{\Delta_c}{L}$$

$$\therefore \frac{\Delta_c}{L} = \left(\frac{\gamma}{2E'\pi a_c} \right)^{1/2}$$

Therefore for a materials with constant elastic constant and critical crack length,

$$\Delta_c \propto L$$

And for the present model, critical displacement (Δ_c) for different domain length is calculated and is plotted below.

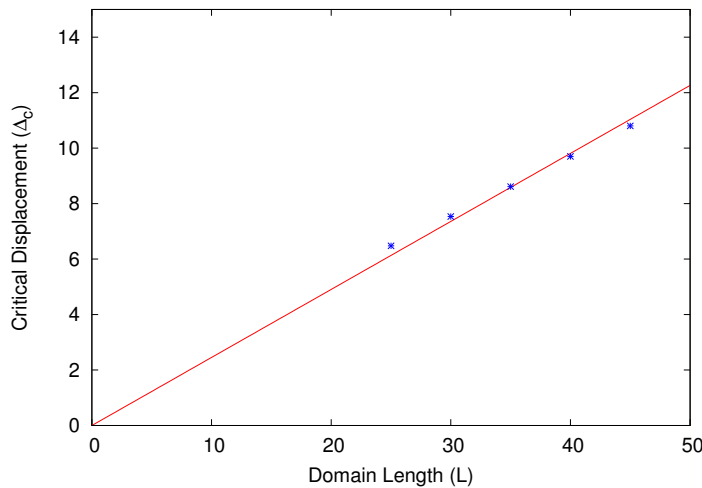


Figure 5.7: Different critical displacement for different domain length.

From the Figure 5.7, it can be seen that the critical displacement varies linearly with the domain size and hence it can be stated that the present model is able to replicate the Griffith's criteria of fracture for brittle material.

5.5 Stress in front of Crack Tip

The stress field around the crack tip for Mode III fracture [7] is given by,

$$\tau_{yz} = \frac{K_{III}}{\sqrt{2\pi r}} \cos\left(\frac{\theta}{2}\right)$$

Now for a system in which steady state crack propagation is taking place at an applied stress of 0.3 units is shown below,

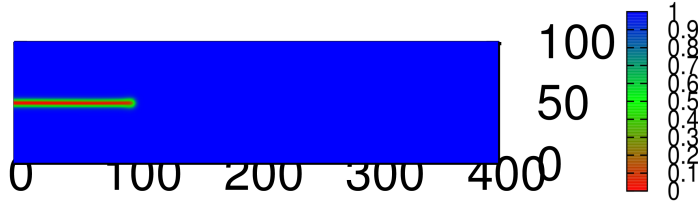


Figure 5.8: Crack propagating in a domain.

The above simulation is carried out under stress controlled conditions.

Now in this domain if a angle of $\theta = 0^0$ is considered and then the stress in front of the crack tip is calculated. The stress profile in front of the crack tip is shown below,

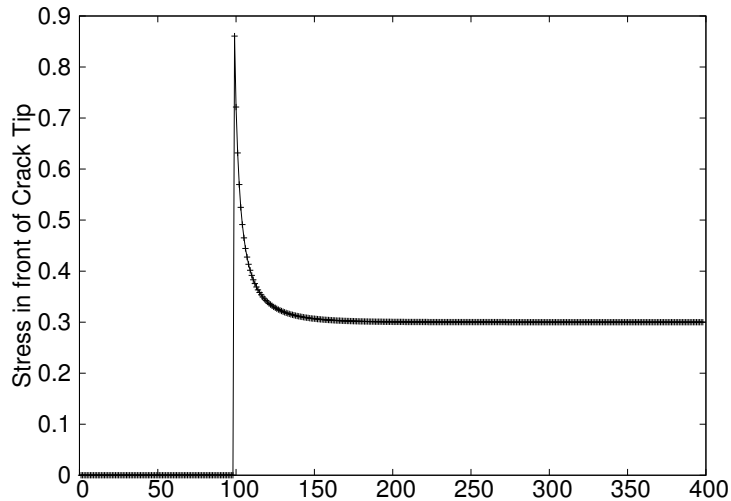


Figure 5.9: Stress in front of the crack tip.

This stress profile (Figure 5.9) is along the line $y = 50$ which overlaps the center of the crack and provide the stress profile which is for an angle of $\theta = 0^0$ from the crack tip. It can be seen that till the point where crack phase is present there is no stress. At the crack tip the stress is maximum because of the stress singularity at the crack tip and it decreases as we move away from the crack tip. The stress in front of crack tip follows the relation shown below,

$$\tau \propto \frac{1}{\sqrt{r}}$$

The stress decreases and finally reaches a constant value far away from the crack tip which is equivalent to the applied stress of 0.3 units.

5.6 Crack Splitting

At significantly higher mobility of the crack-matrix interface, and at higher Δ , the crack can start to split [2] and such a splitting is seen in one of the simulation and is shown below (Figure 5.10).

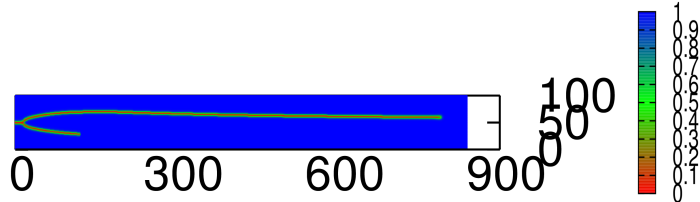


Figure 5.10: Crack splitting at higher applied displacement.

In order to achieve splitting of crack, the initial crack is initiated 5 grid points away from the center. This perturbation is enough to cause the crack to split at higher applied Δ . The same color scheme used in the above figure shows the crack phase in red color, while the matrix is shown by blue color. The interface is shown by green color.

At higher Δ 's, the crack is accelerating, and the strain energy stored in the system is larger than the steadily propagating crack. This higher energy is consumed by creating new surfaces and hence crack branching takes place.

The kinetics of instable crack growth are not studied and further studies have to be done to better understand the branching mechanisms and the differential growth of the crack branches.

5.7 Crack Propagation in systems with different Shear Modulus

Here the crack propagation velocities are compared for systems having different shear modulus. The comparison of the velocities is shown below, (Figure 5.11),

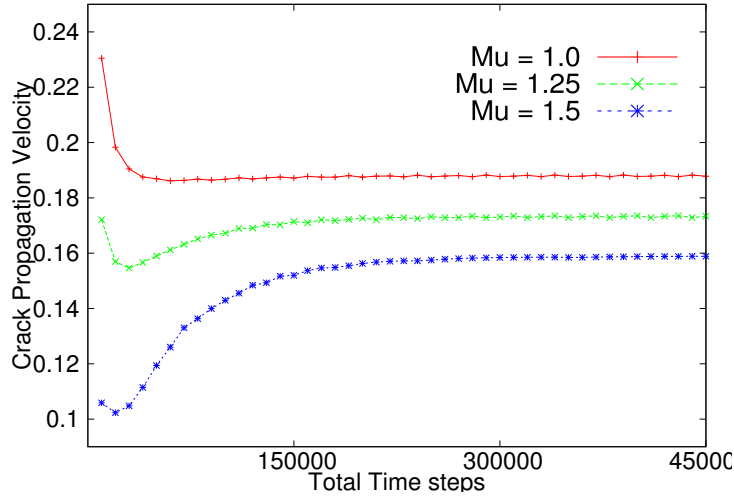


Figure 5.11: Crack propagation velocities comparison in system having different shear modulus.

The above simulation is carried out under stress controlled conditions.

The above graph shows the crack propagation velocities for three different system having shear modulus of $\mu = 1.0$, $\mu = 1.25$, and $\mu = 1.5$ under a constant applied stress of 45 units. Here the red line represents the velocity profile of system having $\mu = 1.0$, the green line represents the velocity profile of system having $\mu = 1.25$ and the blue line represents the velocity profile of system having $\mu = 1.5$. All the three system attain a steady state crack propagation velocity under the present condition as seen in the graph. As the shear modulus increases the crack propagation velocity decreases as the resistance to crack propagation increases. Analytically velocity of crack propagation cannot be obtained from the usual continuum theory without additional assumptions[1]. In the present model we have a consistent theory at both the macroscopic and microscopic scale.

Therefore this model is able to replicate the physics of crack propagation.

5.8 Crack Propagation in Linearly Toughened Material

A domain is made such that the elastic constant (i.e. shear modulus) is linearly increasing in x-direction within the domain. It replicates a situation of linearly toughened material. The shear modulus distribution is shown below (Figure 5.12).

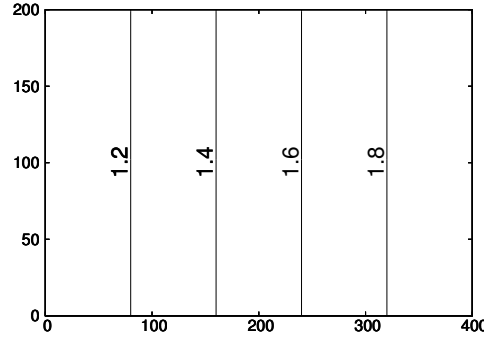


Figure 5.12: Contour plot of linearly increasing shear modulus in the domain.

Figure 5.12 shows the contour plot of the shear modulus. The shear modulus is increasing linearly from a value of 1.0 at the extreme left to 2.0 at the extreme right. Now crack propagation is studied in this linearly increasing shear modulus matrix.

The velocity of crack propagation is studied by initiating the crack at different ends of the matrix. Firstly, the crack is initiated at the extreme left end and is let to propagate in the direction of increasing shear modulus under Mode III fracture condition as shown below (Figure 5.13),

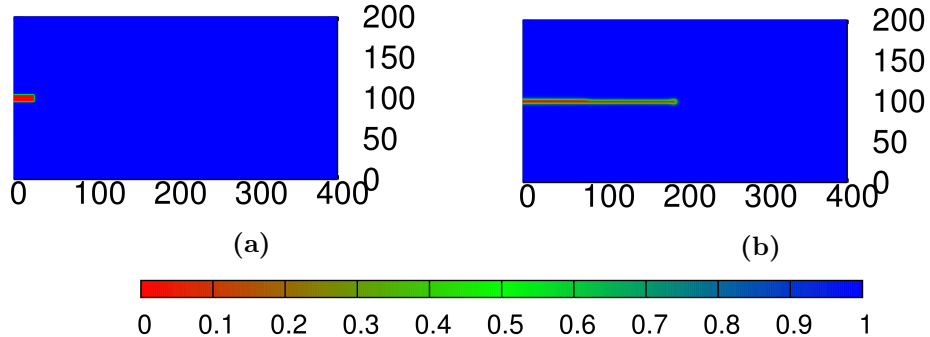


Figure 5.13: a) Initial domain containing a cracks at the left most end of matrix. b) Propagation of the cracks under linear gradient of shear modulus.

It is visible that the crack thickness is decreasing as it propagates as the shear modulus is increasing. And the crack propagation velocity for the above crack propagation is shown below (Figure 5.14),

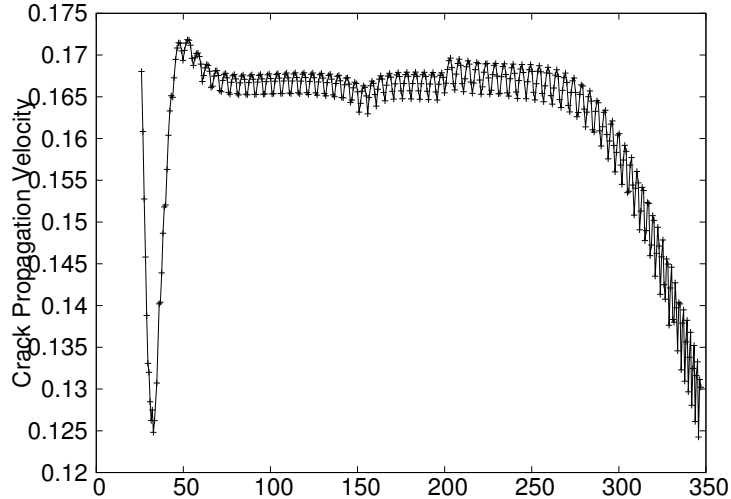


Figure 5.14: Crack propagation velocity for the crack propagating in the direction of increasing shear modulus.

From the above velocity profile it can be seen that the crack propagation velocity is decreasing with increasing shear modulus.

Also now the crack is initiated at the extreme right hand corner and is let to propagate in the direction of decreasing shear modulus under the mode III fracture condition as shown below (Figure 5.15),

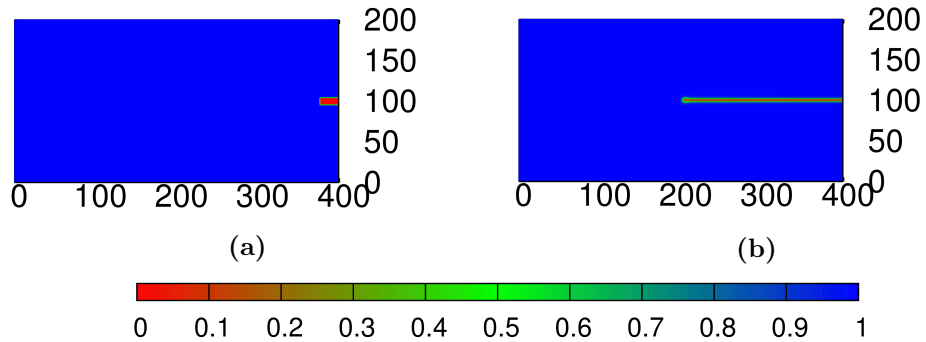


Figure 5.15: a) Initial domain containing a cracks at the right most end of matrix.
b) Propagation of the cracks under linear gradient of shear modulus.

The crack is able to propagate through the matrix in the direction of decreasing shear modulus. The crack propagation velocity for the above crack propagation is shown below (Figure 5.16),

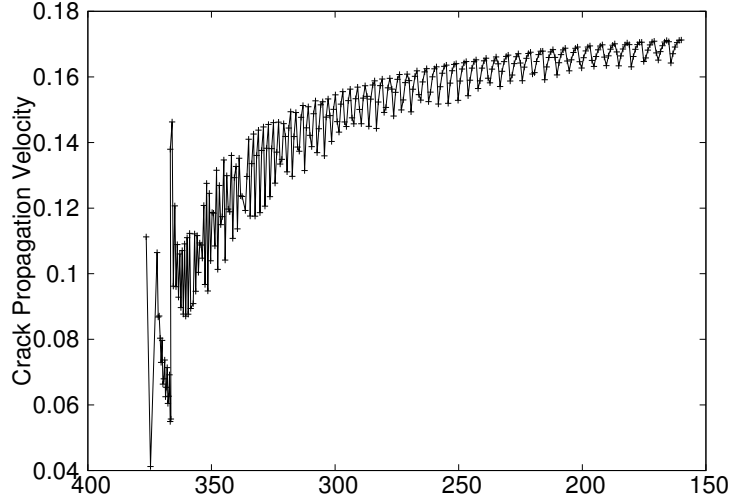


Figure 5.16: Crack propagation velocity for the crack propagating in the direction of decreasing shear modulus.

From the above velocity profile of crack propagation, it can be seen that the velocity of crack propagation is increasing with decreasing shear modulus. These two above observation is consistent with the Griffith's theory, as at a constant stress the crack propagation velocity is higher for a material having lower elastic constant.

5.8.1 Interaction of multiple cracks in the domain

Two cracks are initiated at extreme ends of the domain and are let to interact with each other.

All the simulations were carried out under stress controlled conditions.

A matrix with two cracks at either ends of the domain is stressed under mode III fracture condition, and the crack propagation after certain duration is shown below (Figure 5.17). The applied stress in this particular case is 0.45 units.

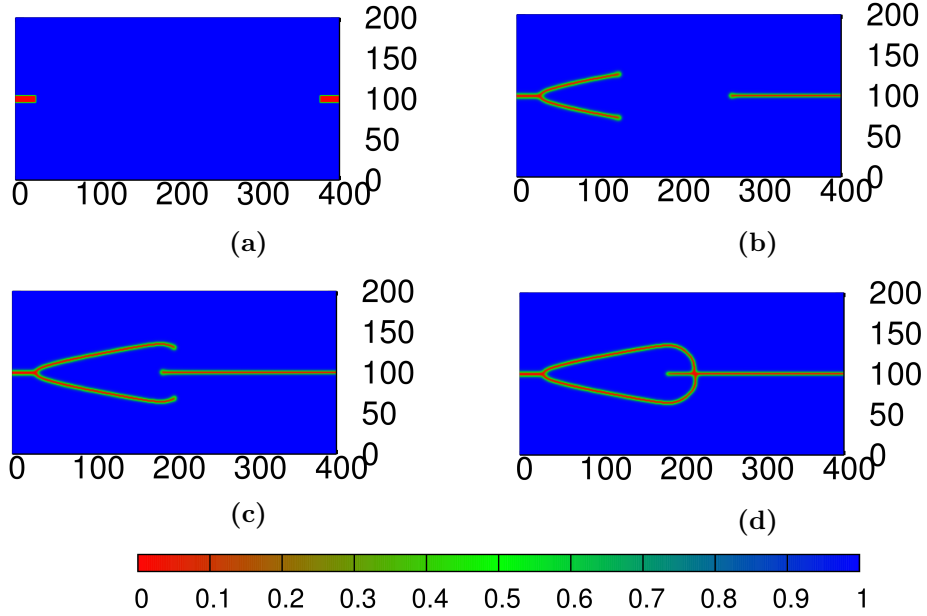


Figure 5.17: Sequence of crack propagation from either end of domain at the applied stress of 0.45 units.

The applied stress is sufficiently high enough to cause the crack splitting at the region on lower shear modulus, i.e. left side crack as shown in Figure 5.17 (b), but is not sufficiently high enough to cause crack splitting at the higher shear modulus region. Also as the crack propagates and the two crack branches come near the strain field of another crack propagating from the right hand side, the crack branches tends to deviate towards the single crack, as shown in Figure 5.17 (c). The strain field interaction of all these three cracks causes the bending of the two branches of the crack, which will eventually lead to crack path minimization.

Finally in order to minimize the total crack path these cracks will merge (Figure 5.17 (d)).

At even higher applied stress of 0.5 units, the crack interaction is shown below (Figure 5.18),

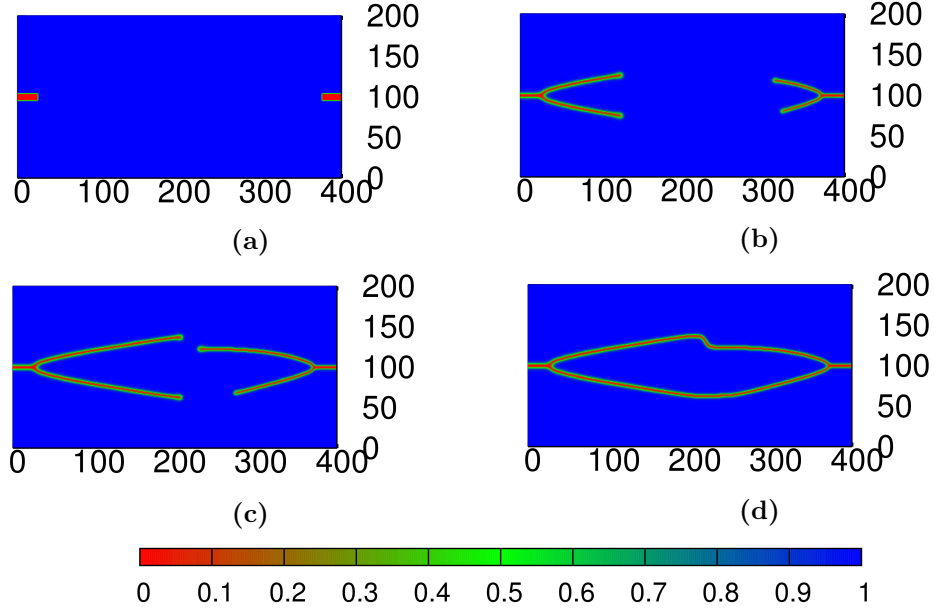


Figure 5.18: Sequence of crack propagation from either end of domain at the applied stress of 0.5 units.

Here the applied stress is sufficiently high enough to cause crack splitting at either end of the domain. But as the shear modulus is higher at the right end, both the crack branches do not have sufficient energy to grow symmetrically, and hence one branch is out grown, Figure 5.18 (b). At later stages the crack merges to minimize the total crack path as shown in the subsequent figures.

The cases below show the crack interaction when the crack are initiated horizontally away from each other. The first case shows crack interaction at an applied stress of 0.4 units.

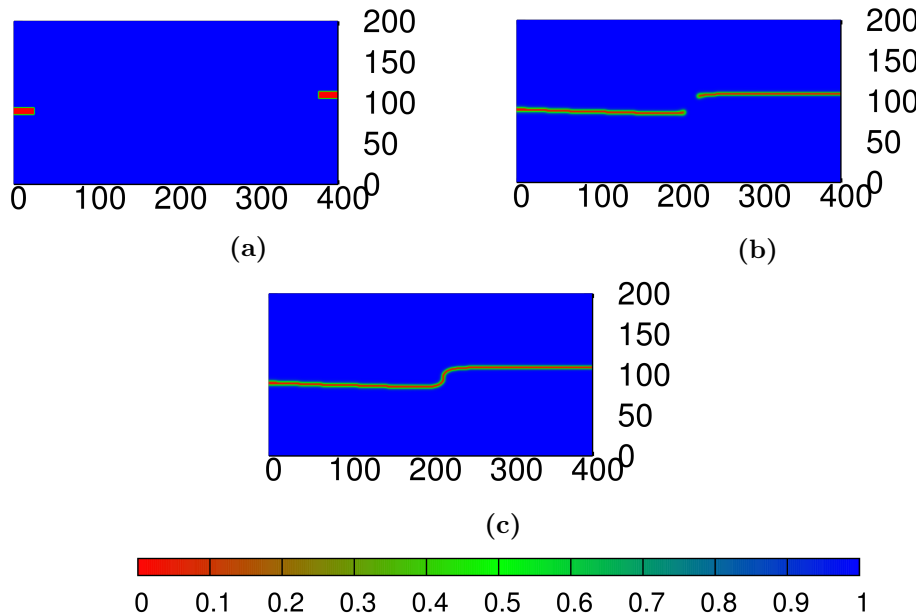


Figure 5.19: Sequence of crack propagation for horizontally away initiated cracks at the applied stress of 0.4 units.

Here the cracks are having differential growth velocity because of the gradient of the shear modulus present in the domain. Also Figure 5.19 (b) shows that the crack tip is bending when the strain field of the two crack comes in the vicinity of one another.

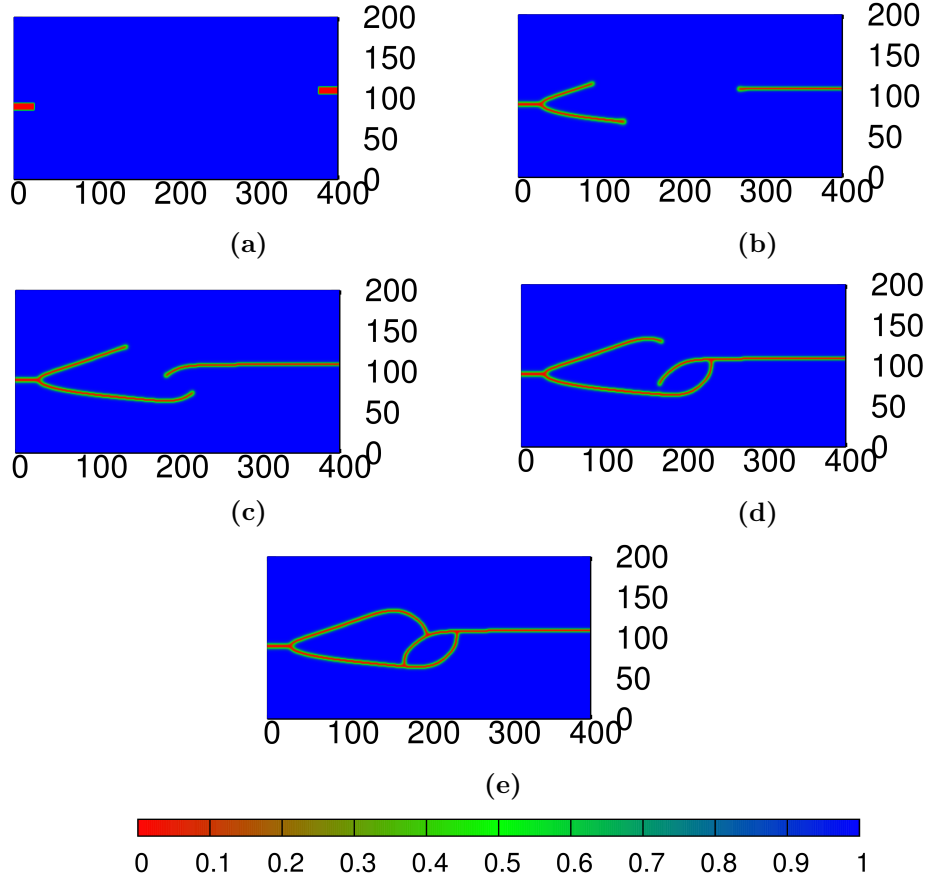


Figure 5.20: Sequence of crack propagation for horizontally away initiated cracks at the applied stress of 0.45 units.

The above case shows the crack splitting at one end due to higher applied stress of 0.45 units. Also the lower branch of the crack starts bending along with the second crack as their strain field comes in vicinity of each other, Figure 5.20 (c). The upper branch of the crack starts bending when its strain field comes in the vicinity of the strain field of the other two interacting cracks, Figure 5.20 (d).

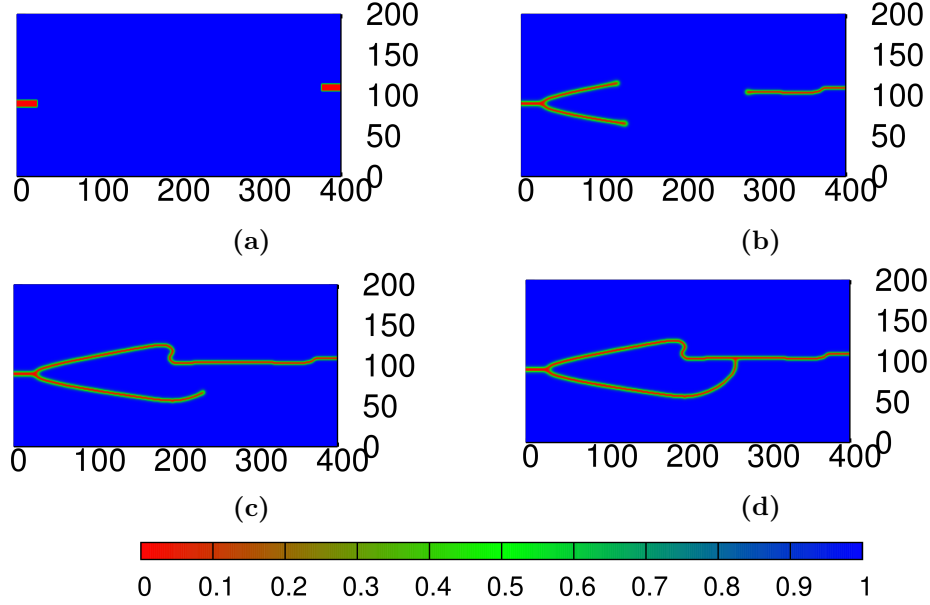


Figure 5.21: Sequence of crack propagation for horizontally away initiated cracks at the applied stress of 0.5 units.

At even higher applied stress of 0.5 units, the crack splitting takes place at both ends, but because of the close vicinity of the boundary and higher shear modulus, one branch of the right hand crack does not sustain, Figure 5.21 (b). Further merging of the three branches of the crack follows.

5.9 Crack Propagation in Anisotropic Domain

The shear modulus of the domain is made anisotropic using the function mentioned below.

$$\mu = \mu_0 a_c^2(\theta)$$

and,

$$a_c = 1 + \delta_{\alpha\beta} \cos 4\theta$$

where $\delta_{\alpha\beta}$ is the strength of anisotropy.

And the polar plot of this anisotropic shear modulus is shown below,

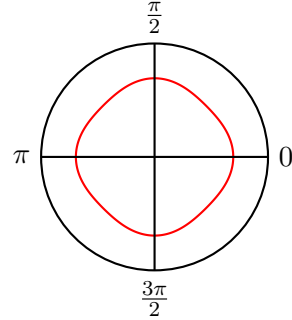


Figure 5.22: Polar plot of anisotropic Shear Modulus.

5.9.1 Constant μ_0

Now to understand the crack propagation in such an anisotropic domain, firstly μ_0 is kept constant at a value of 1.0 and the strength of anisotropy, $\delta_{\alpha\beta}$, is kept constant at a value of 0.02. The crack propagation under the present condition is studied and is shown below,

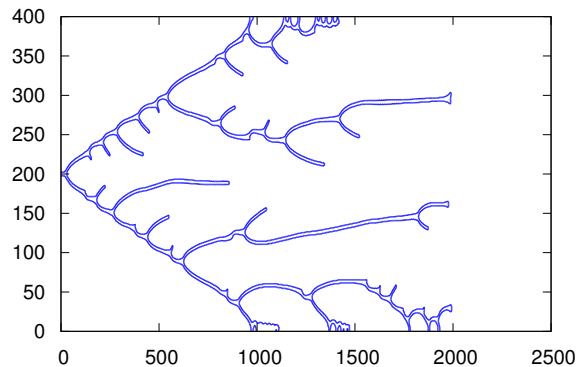


Figure 5.23: Crack branching in anisotropic domain under the applied stress of 0.5 units.

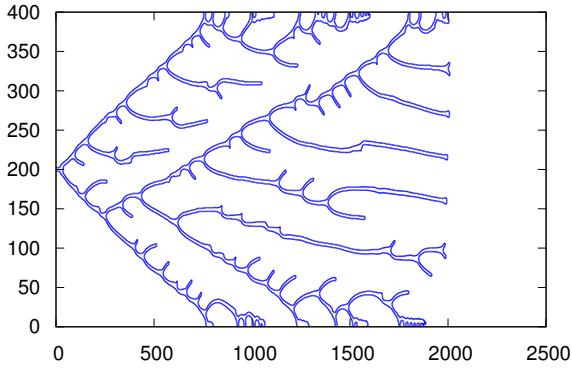


Figure 5.24: Crack branching in anisotropic domain under the applied stress of 0.55 units.

From the above figures it can be seen that the crack tends to propagate in the direction where least resistance is offered to its propagation, where the shear modulus is least. According to the polar plot, the shear modulus is least at about $\pm 45^0$ from the x-axis, and the crack splits in the same direction as seen in the figures above. The branching of crack takes place at the same angle throughout the domain. The crack propagation becomes anisotropic with the shear modulus.

Also as the applied stress increases the extent of crack splitting increases as can be seen from the figures above.

5.9.2 Linearly increasing μ_0

Next, the μ_0 used in the above anisotropic function of shear modulus is made a linear function of x as shown below.

$$\mu_0(x) = 1.0 + 0.005 * x$$

Now the crack propagation in this anisotropic domain is studied by fixing the strength of anisotropy, $\delta_{\alpha\beta}$, to a value of 0.02 and using the linearly increasing $\mu_0(x)$ in the anisotropic shear modulus function. The crack propagation is shown below,

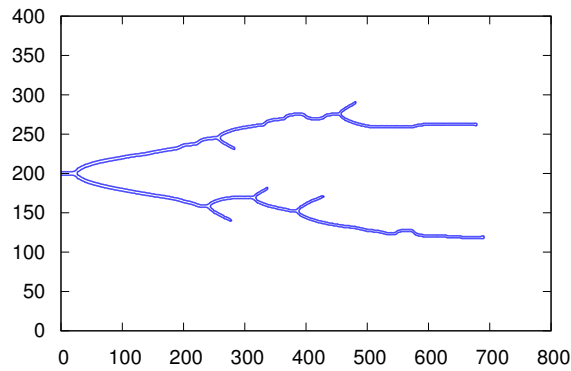


Figure 5.25: Crack branching in anisotropic domain under the applied stress of 0.5 units.

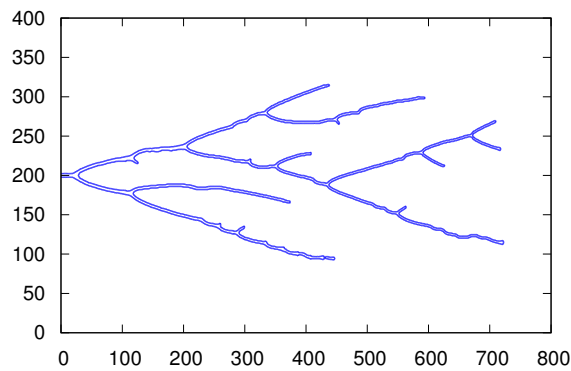


Figure 5.26: Crack branching in anisotropic domain under the applied stress of 0.6 units.

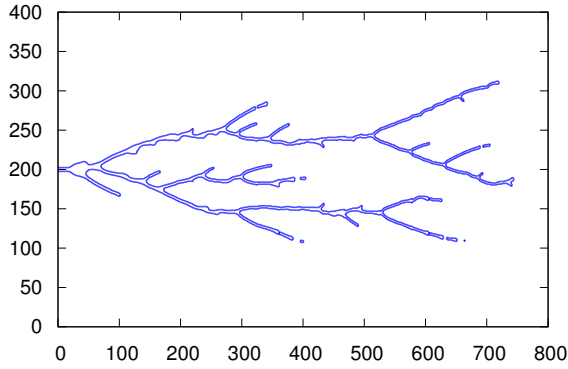


Figure 5.27: Crack branching in anisotropic domain under the applied stress of 0.7 units.

From the above figures it can be seen that the crack is branching out in two main branches at an angle of 45^0 from either side of the initial crack center axis parallel to the x-axis, which offers the least resistance to the crack propagation as described in the model above.

As the applied stress increases from 0.5 units to 0.7 units, it can be seen that the crack branching in the direction of least resistance increases as the amount of strain energy stored is increasing. Also it can be seen that the crack branching phenomenon is decreasing as we move through the x-axis, as the shear modulus is increasing and which increases the resistance to crack propagation.

5.10 Crack Propagation in Multi Grain System

Crack propagation through a multi-grained system is studied in this section. Here different grains are having a different shear modulus which makes them distinct from each other. The crack can follow two different path while propagating through such a system, either through a grain or around a grain. Crack will try to find a path of least resistance and will try to find a path where the shear modulus is least. All the simulation below were carried out under stress controlled conditions. Shown below is the crack propagating through such a system,

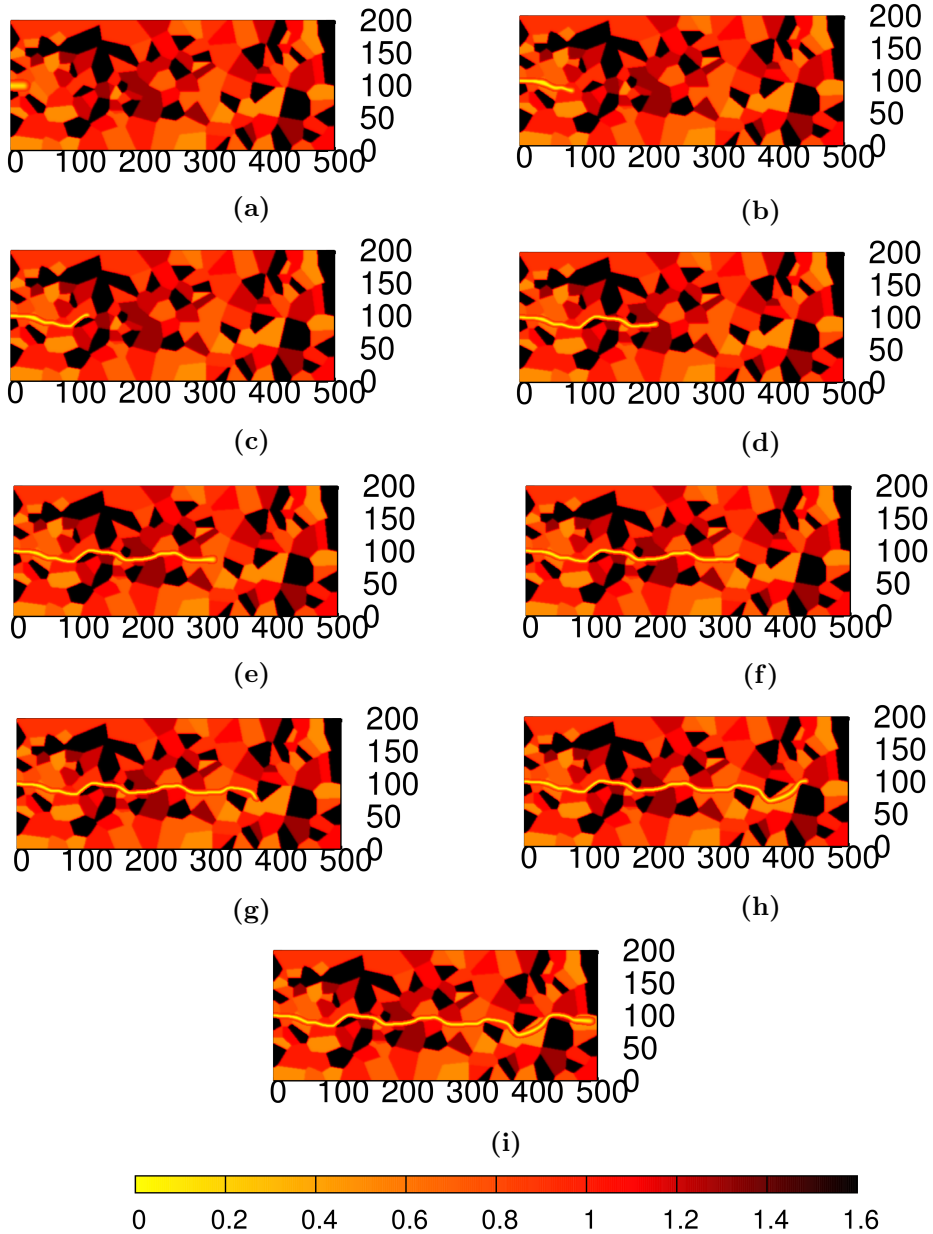


Figure 5.28: Sequence of crack propagating through a multi-grain system.

The above figure (Figure 5.28) shows the path followed by the crack while propagating through the system containing different grains which have different shear modulus. The above system has 150 grains which have shear modulus between 0.6 to 1.6, and different colors are used to distinguish grains with different shear modulus. Yellow color is used to denote the crack phase, whereas reddish-yellow denotes a grain with shear modulus of 0.6 and dark red denotes a grain with shear modulus of 1.4 and as the color changes from reddish-yellow to dark red the shear modulus changes from 0.6 to 1.4. Also the color black denotes a grain with a shear modulus of 1.6. The black color grains are the hardest grains present in the simulation.

Initially as the crack starts to propagates, it propagates through the softer grains (b). Then the crack see a hard grain, it changes its direction in order to move around the hard grain instead of shearing through (c). Again the crack path is such that it avoids the hard grain (d) and then it moves through the domain through and around the grains (e). Again the crack changes its direction to avoid the hard grain and moves through the soft grain, which increases the total crack length inside the system (i) and hence increases the duration of fracture. As seen by the crack path inside this system, the crack is trying to take a path which provides least resistance to its propagation whenever possible as it moves along the matrix.

5.10.1 Crack Splitting around hard grain in Multi-Grain System

The crack propagating through a multi-grain system can have a hard grain in front of its path which can cause the crack to split around the hard grain which is shown below,

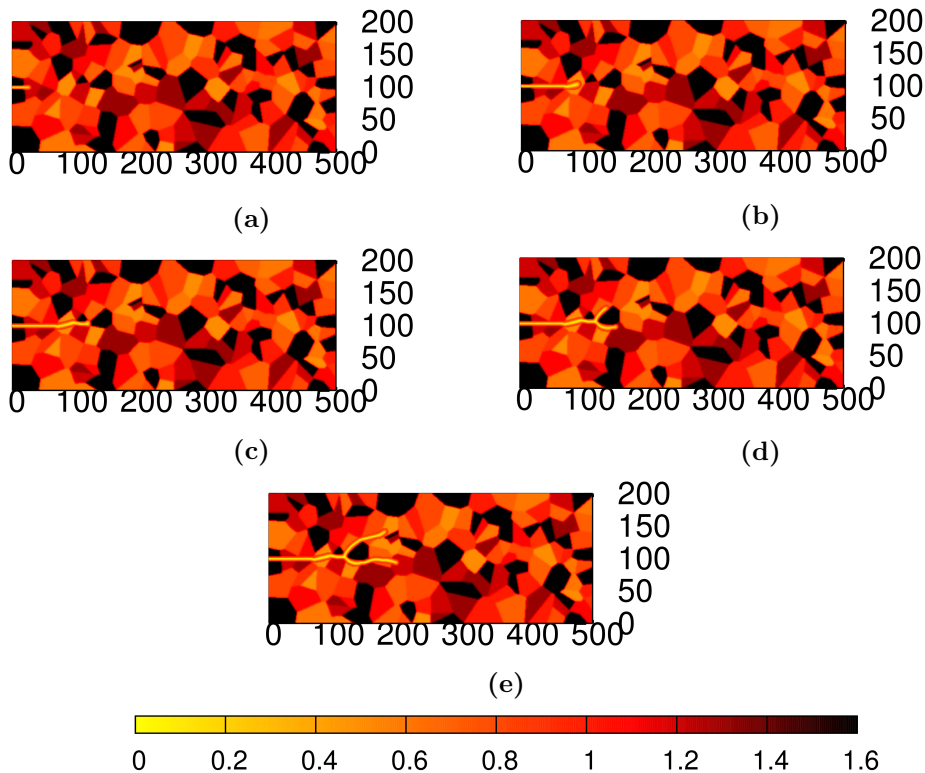


Figure 5.29: Sequence of crack propagating and splitting around a hard grain in a multi-grain system.

The above figure shows a multi-grain domain similar to the above one, where different colors represent different grains with different shear modulus. Yellow color represents crack phase, whereas the color becomes darker from yellow to red the shear modulus

of the grain increases from 0.6 to 1.4 and the color black indicates grain with a shear modulus of 1.6.

Initially as the crack propagates, it moves towards the grain with lower shear modulus away from grains with higher shear modulus (b). Then it avoids the hard grain by moving around it (c). Here the crack comes in contact with the hard grain around which it splits into two branches (d). The stress in front of this hard grain is sufficiently high enough to cause the crack to form two branches and both the branches move around that hard grain and they keep growing (e).

The branching in the above situation sustains and continues to propagate as two independent cracks.

5.10.2 Crack Path blocked by a Hard Grain

Here two cracks are initiated in a multi-grain domain and are propagated under a constant applied stress. The sequence of crack propagation in this system is shown below (Figure 5.30),

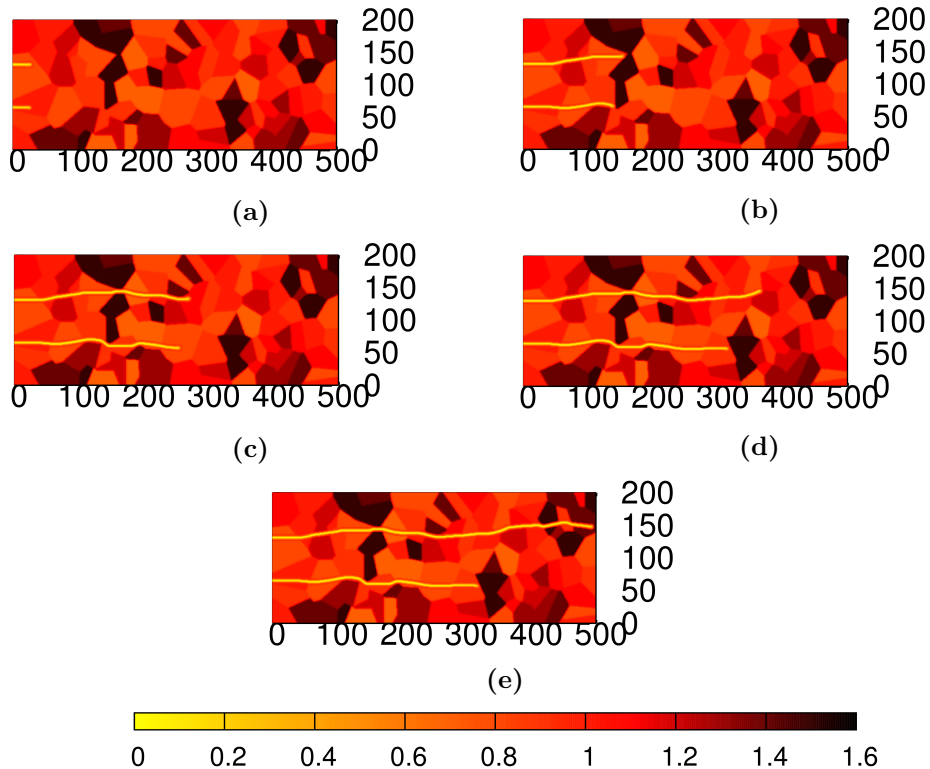


Figure 5.30: Sequence of two crack propagating in a multi-grain system and one crack path is blocked by a hard grain.

The above figure shows a multi-grain domain where different color represents grains having different shear modulus. Yellow color represents the crack phase. And as the color becomes darker from reddish-yellow to dark red, the shear modulus of the grain increases from 0.7 to 1.5, with the dark brown grain having a shear modulus of 1.5, which is the hardest grain.

Initially both the cracks start to propagate through the softer grains. The upper crack is able to move through the small region of hard grain and the lower crack changes its direction to move around the hard grain (b). The cracks move through the softer grains (c), where the lower crack is obstructed in front of the hard grain while the upper crack propagates through the domain (d). The hard grain is sufficiently big enough that the lower crack is unable to shear through it or move around it and it gets blocked by the hard grain whereas the upper crack moves through the domain (e).

5.10.3 Crack Propagation in stacked phases

In order to study the crack propagation in multi-grain system, a new system is designed which contain phases α and β stacked one after another. To study the crack propagation in such system both α and β phases are having different shear modulus. Shown below is the system containing such stacked phases.

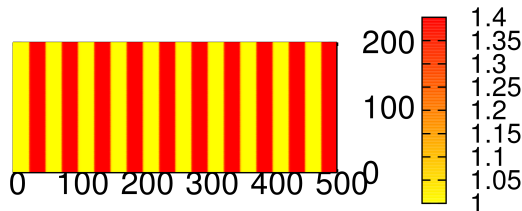


Figure 5.31: Domain containing alternately stacked α and β phases.

The above domain contains alternately stacked α and β phases, where α phase have a shear modulus of 1.0 and β phase have a shear modulus of 1.4. On application of stress the crack propagates through this modified domain. The velocity of crack propagation is shown below,

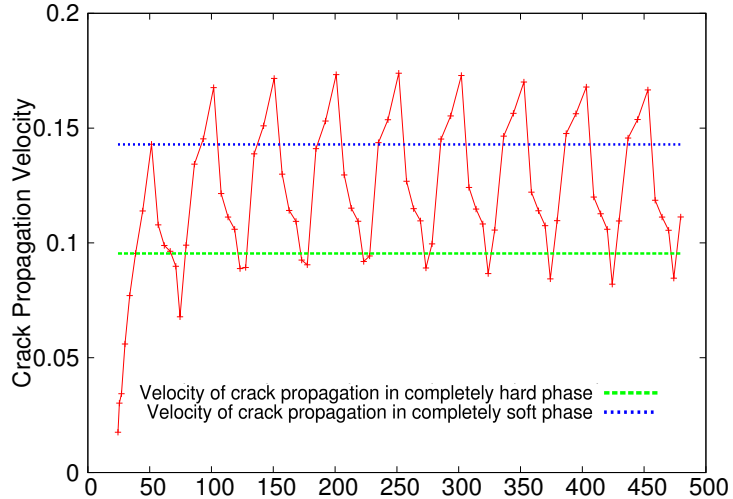


Figure 5.32: The velocity of crack propagation in alternately stacked phases.

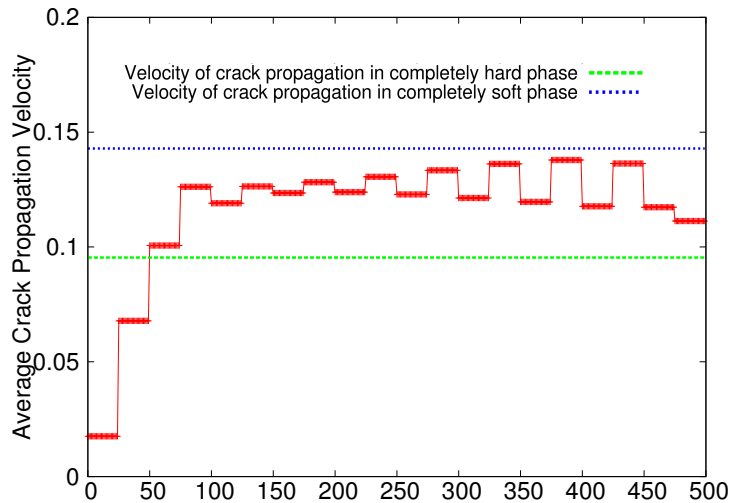


Figure 5.33: The average velocity in a particular phase of the crack propagation in stacked phases.

In the above two graphs the blue line denotes the velocity of crack propagation in a domain containing only β phase having a shear modulus of 1.4 and the green line denotes the velocity of crack propagation in a domain containing only α phase having a shear modulus of 1.0. It can be seen that the velocity of crack propagation near the $\alpha - \beta$ interface is outside the domain of these two reference lines (Figure 5.32). It is because of the stress gradients present in front of the crack tip. But when the average velocity of crack propagation in each phase is plotted (Figure 5.33), the velocity range is within the domain of the two reference lines. This shows that the average velocity of propagation in the present system containing 50% α and 50% β is in between the velocity of crack propagation in pure α and pure β phases.

The velocity of propagation as seen in the graph is varying as we move from one phase to another. But the interesting thing is that the velocity of propagation is lower in β phase having higher shear modulus and lower in α phase having lower shear modulus. This is because of the stress gradient experienced by the crack front at a given time. When the crack is present in the harder phase, it experiences a higher stress gradient as it sees a softer phase ahead of this phase which causes the crack propagation to accelerate and when the crack is in softer phase, it experiences a lower stress gradient as it sees a harder phase ahead of this phase which causes the crack propagation to decelerate. This is because the stress present in the harder grain is higher than present in the softer grain which makes the gradient larger when the crack is present in harder phase and vice versa.

The average velocity of propagation in different phases is almost same (Figure 5.33). The later fluctuation seen in the velocity profile is because of the boundary effect.

Now suppose if the phase fraction is kept constant at 50% α and 50% β , but the thickness of the individual phases is changed in order to find an optimal thickness of the phase so as to maximize the time to fracture or minimize the crack length propagated in a given amount of time of 500000 units. The phase thickness is changed from 125 units to 3 units and the crack length propagated in fixed amount of time is plotted below for a constant applied stress.

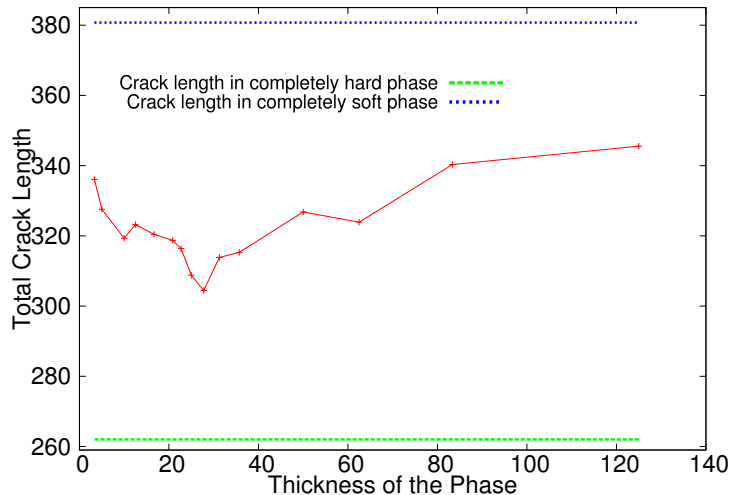


Figure 5.34: The variation of crack length propagated in a fixed amount of time for different thickness of alternate α and β phases.

In the above graph the blue line denotes the crack length propagated in completely hard β phase after 500000 units of time and the green line denotes the crack length propagated in completely hard α phase after 500000 units of time.

It can be seen from the graph that we get a minima at thickness of 28 units. The main reason for this minima to occur is that if the phase thickness is smaller than the decay length of the stress field in front of the crack tip, then the stress field is also seen in the next phase and the desired accelerating-decelerating feature of the crack propagation is lost. And if the decay length of the stress field in front of the crack tip is much smaller than the thickness of the phase, then the stress gradients effects become less effective as the presence of next phase is not felt to the crack tip propagating in one phase. At this particular phase thickness the crack propagation length is minimum, therefore this kind of arrangement can resist the crack propagation to a greater extent.

5.10.3.1 Linearly increasing Shear Modulus of both α and β phase

Here a system is considered in which the α and β phases are alternately arranged and their shear modulus increases linearly as shown in the figure below. But within a given phase the shear modulus remains constant.

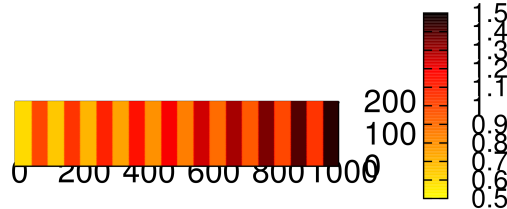


Figure 5.35: Domain containing alternately stacked α and β phases.

The shear modulus of the α phases increases from 0.5 to 0.95 as we move from left to right and the shear modulus of the β phase increases from 1.0 to 1.45 as we move from left to right. And the α and β phases are alternately arranged. The velocity profile of the crack propagation is shown below.

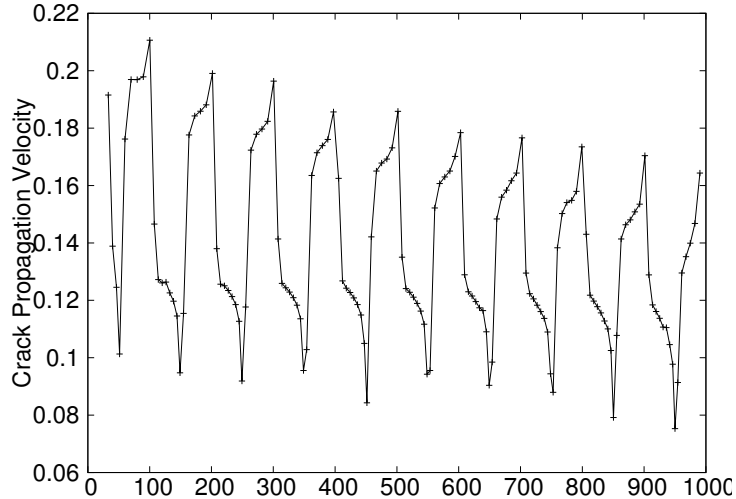


Figure 5.36: The velocity of crack propagation in alternately stacked phases.

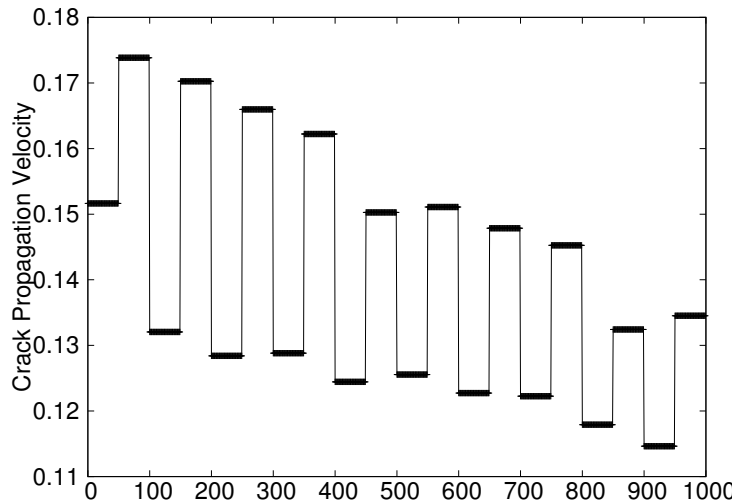


Figure 5.37: The average velocity in a particular phase of the crack propagation in stacked phases.

It can be seen that the velocity profile is decreasing as we are moving from left to right as the shear modulus of both the phases is increasing. Also the average velocity profile is decreasing. But the magnitude of variation of the velocity (Figure 5.36) as it moves from one phase to another remains same as the difference between the shear modulus of the two adjacent phases remains same.

5.10.3.2 Linearly decreasing Shear Modulus of α phase and linearly increasing Shear Modulus of β phase

Here the domain is designed in such a way that the shear modulus of the α phase decreases as we move from left to right and the shear modulus of β phase increases as

we move from left to right. But within a phase the shear modulus remains constant.

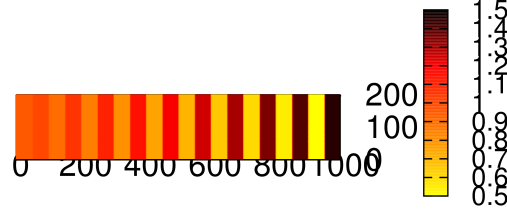


Figure 5.38: Domain containing alternately stacked α and β phases.

The shear modulus of α phase decreases from 0.95 to 0.5 as we move from left to right and the shear modulus of the β phase increases from 1.0 to 1.45 as we move from left to right. The α and β phases are alternately arranged. The velocity profile of crack propagation in such a system is shown below,

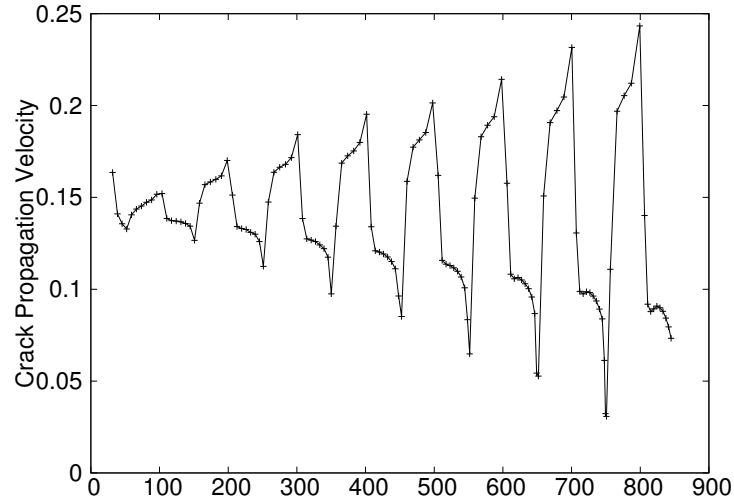


Figure 5.39: The velocity of crack propagation in alternately stacked phases.

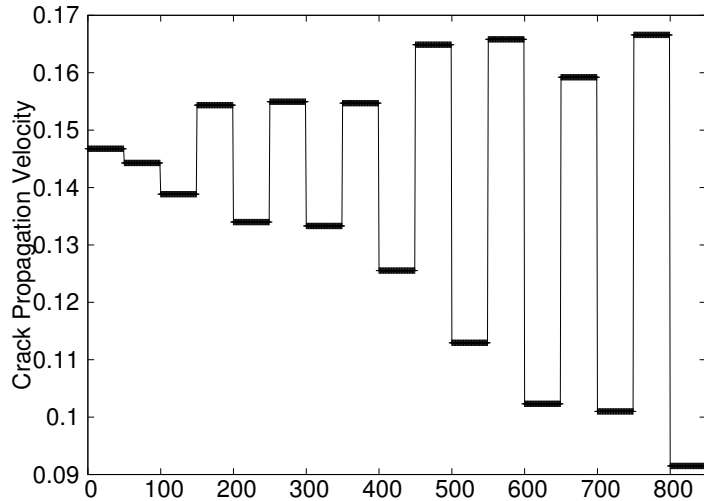


Figure 5.40: The average velocity in a particular phase of the crack propagation in stacked phases.

It can be seen that the velocity profile (Figure 5.39) is having a zigzag profile as the crack propagates through the domain. As the crack moves into a softer phase its velocity goes on decreasing as it moves through it and as the crack propagates through a harder phase its velocity goes on increasing as it move through it. This is due to the difference in stress gradients present in front of the crack tip as it moves from one phase to another. Also the magnitude of fluctuation increases as it moves through the domain. This is because the difference in the shear modulus of the adjacent phases is increasing through the domain.

Also the average velocity profile (Figure 5.40) shows that the average velocity within a hard phase remains almost constant, whereas the average velocity within a softer phase decreases as we move through the domain. The difference between the average velocities within hard and soft phase increases with time as the difference in shear modulus within adjacent grains is increasing.

So it can be seen that the crack propagation in a multi-phase system depends not only on the elastic constants of the phases but it also depends on the environment near the crack front which provides the driving force for the crack propagation. Also it can be extended to a multi-grain system, where the environment will play a much significant role in crack propagation. If the harder grains can be somehow distributed within the domain in such a way the velocity profile of crack propagation becomes move irregular then it will resist the crack propagation to a greater extent.

Chapter 6

Future Work

Other major topic of focus to be covered in this study further are

- Crack propagation under Mode I fracture condition. Also crack propagation under mixed model fracture condition.
- Crack propagating in a anisotropic polycrystalline matrix.

Bibliography

- [1] Alain Karma, David A. Kessler and Herbert Levine, Physical Review Letters 87, 045501 (2001).
- [2] Alain Karma and Alexander E. Lobkovsky, Physical Review Letters 92, 245510 (2004).
- [3] W. J. Boettinger, J. A. Warren, C. Beckermann, and A. Karma, Annual Review of Materials Research 32, 163 (2002).
- [4] L.J. Li, C.H. Lei, Y.C. Shu and J.Y. Li, Acta Meterialia 59, 2648 (2011).
- [5] S. M. Allen and J. W. Cahn, Acta Meterialia 20, 423 (1972).
- [6] A.A. Griffith Philosophical Transactions of the Royal Society of London A 221, 163 (1921).
- [7] Brian Lawn, *Fracture of brittle solids (2nd ed.)*, (Cambridge University Press, 1993).
- [8] William H Press, Saul A. Teukolsky , William T. Vetterling and Brian P. Flannery, *Numerical Recipes: The Art of Scientific Computing (3rd ed.)*, (Cambridge University Press, 2007).
- [9] Atsuyuki Okabe and Kokichi Sugihara, *Spatial Tessellations: Concepts and Applications of Voronoi Diagrams (2nd ed.)*, (Wiley, 2008).